



UNIVERSITY OF LEEDS

This is a repository copy of *Reynolds number dependence of particle resuspension in turbulent duct flows*.

White Rose Research Online URL for this paper:
<http://eprints.whiterose.ac.uk/130415/>

Version: Accepted Version

Article:

Zhao, YL, Wang, Y, Yao, J et al. (1 more author) (2018) Reynolds number dependence of particle resuspension in turbulent duct flows. *Chemical Engineering Science*, 187 (1). pp. 33-51. ISSN 0009-2509

<https://doi.org/10.1016/j.ces.2018.04.053>

(c) 2018 Elsevier Ltd. All rights reserved. Licensed under the Creative Commons Attribution-Non Commercial No Derivatives 4.0 International License (<https://creativecommons.org/licenses/by-nc-nd/4.0/>).

Reuse

This article is distributed under the terms of the Creative Commons Attribution-NonCommercial-NoDerivs (CC BY-NC-ND) licence. This licence only allows you to download this work and share it with others as long as you credit the authors, but you can't change the article in any way or use it commercially. More information and the full terms of the licence here: <https://creativecommons.org/licenses/>

Takedown

If you consider content in White Rose Research Online to be in breach of UK law, please notify us by emailing eprints@whiterose.ac.uk including the URL of the record and the reason for the withdrawal request.



eprints@whiterose.ac.uk
<https://eprints.whiterose.ac.uk/>

Reynolds number dependence of particle resuspension in turbulent duct flows

Yanlin Zhao¹, Yanzhi Wang¹, Jun Yao^{1*}, Michael Fairweather²

¹Beijing Key Laboratory of Process Fluid Filtration and Separation, College of Mechanical and Transportation Engineering, China University of Petroleum-Beijing, Beijing 102249, People's Republic of China

²School of Chemical and Process Engineering, University of Leeds, Leeds, LS2 9JT, UK

* Corresponding Author:

Prof. Jun Yao, College of Mechanical and Transportation Engineering, China University of Petroleum-Beijing, Beijing 102249, People's Republic of China

Telephone: +86 (0) 10 89733266; Facsimile: +86 (0) 10 89733658; Email address:
yaojun@cup.edu.cn

Abstract

Particle resuspension in a fully developed turbulent square duct flow is simulated using one-way coupled large eddy simulation coupled with a Lagrangian particle tracking technique for a range of bulk Reynolds numbers ($36.5k$, $83k$ and $250k$) and four particle sizes ranging from 5 to $500\mu m$ ($St=0.01\sim 2415$) considered. Results obtained for the single-phase flow show good agreement with experimental data. Predictions of the time-dependent particle-laden flows demonstrate that the secondary flow mainly dominates particle resuspension in the regions near the center and sidewalls of the duct. It is found that particle resuspension decreases with particle size. The smaller particles tend to be more prone to resuspension, and are resuspended for a longer duration than larger particles. The mean particle resuspension velocity is found to increase with the duct height. In addition, particle resuspension in the vertical direction increases with Reynolds number while the effect of particle size on particle resuspension decreases. The resuspension rate in the spanwise direction fluctuates more as the Reynolds number increases. It is also found that the average particle resuspension rate in the lower half of the duct is always close to 0.5 , and is independent of time, particle size and Reynolds number. Based on a dynamic analysis, the drag force is found to dominate the resuspension of small particles, while the lift force tends to dominate particle resuspension with increasing particle size. For low Reynolds number ($36.5k$ and $83k$) flows, the drag force plays an important role in the upper regions of the lower half of the duct, but the lift force dominates particle behaviour in the lower regions. It can be concluded that the effects of duct height on particle behaviour decline significantly with Reynolds number.

Key words Particle resuspension; Turbulence; Reynolds number; Duct flow; Secondary flow

1. Introduction

Particle resuspension in turbulent flows in close proximity to solid surface occurs in many environmental and industrial applications. Cleaning of electronic chips, handling of powders, oil and gas production, ventilation systems, diseases transmission, pneumatic conveying, pesticide transportation (Sehmel, 1980; Middleton, 1981; Nicholson, 1988; Soepyan et al. 2016) are just a few examples. Understanding of particle behavior in these processes is of great significance to the design and operation of related equipment (Chen et al. 2013; Zhang et al. 2008). In addition, nuclear waste often exists in the form of liquid-solid sludges which are prone to form solid beds and can lead to the blockages in pipes and equipment, although this can be avoided by keeping the particles in a suspended state during their transportation. Further understanding of particle resuspension thus provides important input to safety assessments of equipment handling solid-liquid flows.

In the past half century, a number of researches concerning turbulent single-phase flows within square ducts have been conducted, including experimental investigations (Brundrett and Banines, 1964; Launder and Ying, 1972; Melling and Whitelaw, 1976), direct numerical simulation (DNS) (Gavrilakis, 1992; Pinelli et al., 2010) and large eddy simulation (LES) (Madabhushi and Vanka, 1991; Huser and Biringen, 1993; Yao et al., 2015). However, there have only been a relatively few numerical studies of particle-laden turbulent flows in square ducts to date. Winkler et al (2004) studied the preferential concentration of particles in a fully developed turbulent vertical square duct flow with $Re_b=5810$ (based on the mean friction velocity and duct width) using LES, finding that particles tended to accumulate in regions of high strain-rate and low swirl strength. Additionally, they further analyzed the relative importance of the lift force on large particles due to the presence secondary flows in the same square duct flow in their later work (Winkler et al, 2009). Sharma and Phares (2006) used DNS to investigate the effect of the secondary flows on the dispersion of particles suspended in a

turbulent square duct flow for $Re_b=5810$, where it was found that high inertia particles accumulate close to the wall and tend to mix more efficiently in the streamwise direction. Fairweather and Yao (2009) conducted the similar investigations at a higher Reynolds number ($Re_b=250K$) using LES. Zhang and Li (2008) applied the Reynolds-averaged Navier-Stokes (RANS) approach with a Reynolds stress turbulence model to study particle deposition in a horizontal turbulent flow, considering particle deposition not only on the duct floor but also on the vertical walls and the ceiling of the duct. Similarly, Yao and Fairweather (2010) studied the behavior of particle resuspension in a turbulent horizontal square duct flow ($Re_b=250k$) using LES combined with a Lagrangian particle tracking technique, with the study focusing on the effect of turbulence-driven secondary flows on the resuspension process. Later, the same authors (Yao and Fairweather, 2012) studied the particle deposition in flows spanning a wide range of Reynolds number ($Re_b=10320, 83k, 250k$). In addition, Adams et al. (2011) compared the results of RANS-based predictions with LES for calculating particle deposition and resuspension in square duct flows at $Re_b=250k$ and concluded that both techniques are consistent in terms of their predictions of particle dispersion and deposition, but that the RANS method predicts a higher variable resuspension rate than LES across the duct. More recently, Zhang et al (2015) studied the effect of collisions on particle behavior in a fully developed square duct flow based on DNS, finding that inter-particle collisions influence the particle resuspension rate near the duct floor, whereas they have a negligible effect on particle behavior near the duct center (in the case of where the effect of gravity was considered).

Particle resuspension mechanisms in turbulent square duct flows have received limited attention, although in recent years there have been a number of studies of particle resuspension behavior in channel flows and wall-bounded flows. Fu et al (2013) developed a stochastic model to predict particle resuspension in a wall-bounded turbulent flow, emphasizing the importance of the particle rolling mechanism on the resuspension process. Barth et al (2014)

conducted experimental tests to investigate particle resuspension in a horizontal turbulent channel flow at $Re_b=8900$ and found that particle resuspension occurs when the fluid friction velocity reaches a critical level, with lower fluid velocities required by large particles than by small particles. In 2015, they further investigated particle deposition and resuspension behavior in gas-cooled reactors (Barth et al. 2015). In addition, Afkhami et al (2014, 2015) employed LES and the discrete element method to study particle dispersion and agglomeration behavior in a horizontal channel flow and concluded that both particle-particle interactions and Reynolds number have a significant effect on these particle behaviors across the flow Re_b range considered (2100-8260). Li et al. (2016) also used direct numerical simulation to study particle-flow turbulence interaction in the wall region of a flat plate boundary layer. In summary, previous studies have focused on particle resuspension in turbulent flows other than ducts, and the behavior of particles in the latter geometry would be expected to be different from that in previous studies due to the secondary flows that occur in a duct.

Previous work by Yao and Fairweather (2010) investigated particle resuspension in a turbulent duct flow at a single Reynolds number ($250k$). However, the mechanisms responsible for particle resuspension within turbulent duct flows at various Reynolds numbers have not been studied. The present work therefore focuses on the mechanisms of resuspension with variations in the flow Reynolds number, considering the effects of the secondary flow, lift force, particle size and duct height. In this paper, the first section provides an introduction to the work and some background; the second section introduces the mathematical models employed, including large eddy simulation and Lagrangian particle tracking; and the third section presents the results and discussion, including flow field validation, flow analysis, consideration of particle resuspension mechanisms and a dynamic analysis. Finally, the fourth section covers conclusions that arise from the work performed.

2. Mathematical model

2.1 Flow configuration

A schematic diagram of the square duct used in present work is given in Fig.1. A three-dimensional Cartesian co-ordinate system(x, y, z) is used to describe the duct flow where the z axis aligns with the streamwise direction, the y axis the spanwise direction and the x axis the vertical direction. The corresponding velocity components in the (x, y, z) directions are (u, v, w) , respectively. To predict this flow, no-slip and periodic boundary conditions were applied at the duct boundary walls, and at the inlet and outlet of the duct, respectively. In addition, the streamwise pressure gradient was considered to drive the flow dynamically to maintain a constant mass flux through the duct.

The size of the duct was $h \times h \times 4\pi h$ in x, y and z direction, respectively. The number of grid nodes used to discretize the physical domain ranged from 4.5×10^5 to 1.44×10^6 across the Reynolds number range considered. Compared with the 2.0×10^6 grid nodes used by Huser and Biringen (1993) in their DNS study, the present LES simulations may be considered highly resolved, with comparisons in the present work between results derived on the basis of the maximum number of nodes noted above and approximately 75% of that number indicating that the unresolved sub-grid scale had little effect on the particle statistics presented in the next section. The length of the duct was sufficiently long to accommodate the streamwise-elongated, near-wall structures present in wall-bounded shear flows, with such structures rarely expected to be longer than approximately 1000 wall units (Robinson and Chow, 1991). Uniform grids were applied in the streamwise direction, and non-uniform grids were used in the vertical and spanwise direction, where the grid points were clustered towards the walls. For all simulation cases, the distance between the first grid node and the walls was x^+ or $y^+ = 0.37 \sim 6.39$, with an average of 5 nodes in the near-wall regions (x^+ or $y^+ < 10$). In addition, sensitivity studies on the numerical grid distribution and the numbers of computational nodes

were also conducted to demonstrate that the final grid arrangement selected gave turbulence statistics that were independent of these parameters.

The flows investigated in present work had bulk Reynolds numbers, $Re_b = w_b h / \nu$ of $36.5k$, $83k$ and $250k$, defined using the duct width and area-averaged streamwise velocity, with corresponding approximate friction Reynolds number, $Re_\tau = u_\tau h / \nu$ of 1990 , 3860 and 10550 , which also can be determined using the empirical relationship for square duct flows proposed by Jones (1976):

$$\frac{1}{\sqrt{f}} = 2 \log(1.125 Re_b \sqrt{f}) - 0.8 \quad (1)$$

where f is the friction factor, defined as $f = 8u_\tau^2 / w_b^2$, and u_τ is the friction velocity (defined as $u_\tau = \sqrt{\tau_w / \rho_f}$, where τ_w is the mean wall shear stress and ρ_f is the fluid density)

2.2 Large eddy simulation

Large eddy simulation was applied in the present work to predict the duct flows for the different Reynolds number cases described above. LES only computes the large energetic scales of motion directly with the small scales modelled (Smagorinsky, 1963). A top-hat filter (Germano, 1992), implemented through finite-volume implicit grid-filtering, was applied to the Navier-Stokes equations for an incompressible Newtonian fluid with constant properties. Under the assumption that filtering and differentiation in space commute, the equations of fluid motion are:

$$\frac{\partial \bar{u}_j}{\partial x_j} = 0 \quad (2)$$

$$\frac{\partial \bar{u}_i}{\partial t} + \frac{\partial \bar{u}_i \bar{u}_j}{\partial x_j} = - \frac{\partial \bar{p}}{\rho \partial x_j} - \frac{\partial}{\partial x_j} (\bar{\sigma}_{ij} + \tau_{ij}) \quad (3)$$

In Eq. (3), $\bar{\sigma}_{ij}$ is the kinematic viscous stress tensor, and τ_{ij} represents the transportation of momentum between the sub-grid scale (SGS) and the resolved scales, and this term, known as the sub-grid scale stress, must be modelled to solve the filtered equations.

Here, the dynamic SGS stress model of Germano et al. (1991) was adopted, which is implemented by using the localization procedure of Piomelli and Liu (1995) with the modifications proposed by di Mare and Jones (2003). In this model, the anisotropic part of the SGS stresses can be obtained from:

$$\tau_{ij}^a = -2(C\Delta)^2 \|\bar{s}\| \bar{s}_{ij}^a \quad (4)$$

where \bar{s}_{ij} is the resolved strain tensor, and Δ is the filter width.

To evaluate the parameter C , a second filtering operation using the test-filtered grid is applied to Eq.(3), and the obtained SGS stresses are:

$$T_{ij} = \bar{u}_i \bar{u}_j - \tilde{u}_i \tilde{u}_j \quad (5)$$

where the tilde denotes application of the second filtering operation. According to the Germano (1991, 1992) identity:

$$L_{ij} = T_{ij} - \tilde{\tau}_{ij} = \bar{u}_i \bar{u}_j - \tilde{u}_i \tilde{u}_j \quad (6)$$

The parameter C can then be evaluated through the relation between the model constant values C and $C^2 \tilde{\Omega}$ at the grid- and test-filter levels, respectively, giving the expression proposed by di Mare and Jones (2003):

$$C^2 \tilde{\Omega} = C^2 \left(1 + \frac{\varepsilon}{2\sqrt{2}\tilde{\Delta}^2 \|\tilde{s}\| \|\tilde{s}^a\|^2} \right) \quad (7)$$

where $\varepsilon \approx v^3/l$ has the dimensions of dissipation under the assumption that the flow has only one length scale l and velocity scale v .

Eq. (7) is based on the hypothesis that the scale invariance of C can be invoked only if the cut-off falls inside the inertial sub-range, with the modelled dissipation representing the entire dissipation in the flow. However, due to the high Reynolds number limit, the dissipation can be only determined by v and l so that the ratio of ε to $\tilde{\Delta}^2 \|\tilde{s}\|^3$ is a measure of how far the flow is from scale preserving conditions. This equation is a first-order expansion of other scale-dependent expressions for C , e.g. that of Porte-Agel et al.(2000). Contracting the tensor \tilde{s} on both sides of Eqs. (6) and (7), then gives:

$$C^2 = \frac{[2\sqrt{2}(C_*^2 \Delta)^2 \|\bar{s}\| \|\bar{s}_{ij}^a\| \|\tilde{s}_{ij}^a - L_{ij}^a \tilde{s}_{ij}^a\|]}{\varepsilon + 2\sqrt{2} \tilde{\Delta}^2 \|\bar{s}\| \|\tilde{s}^a\|^2} \quad (8)$$

where C_*^2 is a provisional value for C^2 , e.g. its value at the previous time step, as used by Piomelli and Liu (1995). The main advantage of this method is that it is well conditioned and avoids the spiky and irregular behavior exhibited by some implementations of the dynamic model and, if the resolved strain tends to zero, C^2 also tends to zero, while $C^2 \tilde{\Omega}$ remains bounded. Eq. (7) also yields smooth C^2 fields without the need for averaging, and the maxima of C^2 are of the same order of magnitude as Lilly's (1967) estimate for the Smagorinsky model constant. However, Eq. (7) cannot prevent negative values of the model parameter, with such values set to zero to prevent instability. Negative values of the SGS viscosity are similarly set to zero. Test filtering was performed in all space directions, with no averaging of the computed model parameter field. The ratio $\tilde{\Delta}^2/\Delta$ was set to 2 and the filter width determined from $\Delta = (\Delta_x \Delta_y \Delta_z)^{1/3}$.

The fluid field computations used the computer program BOFFIN, which implements an implicit finite-volume incompressible flow solver. Due to its co-located storage arrangement, fourth-order pressure smoothing was applied to prevent oscillations in the pressure field. An implicit Gear method was used for time advancement of all transport terms, and the overall procedure is second-order accurate in space and time. The time step was constant with the maximum of the Courant number lying between 0.1 and 0.3. This code has been verified by many previous LES studies for a wide range of flows, such as plane and jets flow (Jones and Wille, 1996), flows over fences (Di Mare and Jones, 2003), particle flows (Fairweather and Yao, 2009, 2012) and turbulent flows in ducts (Yao et al, 2015). Further details of the code and the numerical methods within it can be found in Wille (1997) and Di Mare (2002).

2.3 Lagrangian particle tracking

In this work, the volume fraction of the dispersed phase is low enough ($\leq 10^{-5}$) (Elghobashi, 1994) that the one-way coupling approach is reasonable because the suspended particles are small in size compared to the Kolmogorov length scale of the flow, and because of the low mass loading. Many numerical simulations of multiphase flows have considered only one-way coupling effects for similar reasons (Squires and Eaton, 1991; Rouson and Eaton, 2001; Wang and Squires, 1996). A Lagrangian approach (Fan, et al. 2002; Yao, et al. 2009) was applied to model the particle motion, in which the particles were followed along their trajectories through the unsteady, nonuniform flow field. In order to simplify the analysis, the following assumptions were made: (i) the particle-laden flow is dilute, and interactions between particles are negligible, (ii) the flow and particles are one-way coupled, which means the effect of the particles on the fluid is neglected, and (iii) all particles are rigid spheres with the same diameter and density, and particle-wall collisions are elastic. According to the above hypothesis, the Lagrangian particle motion equation is:

$$\frac{d\mathbf{u}_p}{dt} = \frac{3}{4} \frac{\rho_f}{\rho_p} \frac{C_D}{d_p} (\mathbf{u} - \mathbf{u}_p) |\mathbf{u} - \mathbf{u}_p| + \left(1 - \frac{\rho_f}{\rho_p}\right) \mathbf{g} + 1.615 d_p \mu_f Re_s^{0.5} c_{ls} \frac{[(\mathbf{u} - \mathbf{u}_p) \times \boldsymbol{\omega}_f]}{|\boldsymbol{\omega}_f|} \quad (9)$$

where \mathbf{u} is the fluid velocity, ρ_f is the fluid density, \mathbf{u}_p is the particle velocity, ρ_p is the particle density, d_p is the particle diameter, \mathbf{g} is gravitational acceleration, $\boldsymbol{\omega}_f = 0.5 \nabla \times \mathbf{u}$ is the fluid rotation, $Re_s = \rho_f d_p^2 |\boldsymbol{\omega}_f| / \mu_f$ is the particle Reynolds number of the shear flow, and c_{ls} represents the ratio of the extended lift force to the Saffman force, according to:

$$c_{ls} = \begin{cases} 0.0524 (\beta Re_p)^{0.5}, & Re_p > 40 \\ (1 - 0.3314 \beta^{0.5}) e^{-\frac{Re_p}{10}} + 0.3314 \beta^{0.5}, & Re_p \leq 40 \end{cases} \quad (10)$$

Here, β is a parameter given by $\beta = 0.5 Re_s / Re_p$ (for $0.005 < \beta < 0.4$), and C_D is the Stokes coefficient for drag, $C_D = (1 + 0.15 Re_p^{0.687}) 24 / Re_p$, where Re_p is the particle Reynolds number, $Re_p = d_p |\mathbf{u} - \mathbf{u}_p| / \nu$. The third term on the right hand side of Eq. (9) is the slip-shear force that is based on the analytical result of Saffman (1965, 1968) and extended for

higher particle Reynolds numbers according to Mei (1992). It should be noted that only particles 1.5 times their diameter away from the duct floor are considered, and the drag and lift coefficients are well described using the above expressions based on the work of Zeng and Balachandar (2009), in which the near-wall effect on drag and lift coefficient was investigated in a linear shear flow.

There are a number of possible forces acting on a particle, but most can be neglected due to their minimal effect on the accuracy of the predictions, depending on the particle inertia. In this work, Stokes drag, gravity, buoyancy, and lift forces were considered, in line with Eq. (9). In addition, electrostatic charge may be generated on the particle surface and the duct wall due to particle-wall impaction (Yao et al., 2004), but the electrostatic force acting on a particle can be neglected because its value is much lower than that of the gravity effect by at least two orders of magnitude (Yao et al., 2006). Other forces acting on a particle, including the hydrostatic force, Magnus effect, Basset history force, and added mass force, were not taken into account due to their being orders of magnitude lower than the other forces considered (Armenio and Firorotto, 2001).

The particle equation of motion (Eq. (9)) was solved using a fourth-order Runge–Kutta scheme, given the initial particle location and velocity. The initial particle positions were distributed randomly throughout the duct, and the initial particle velocity was set equal to the local fluid velocity, interpolated to the particle position. Particles were assumed to interact with turbulent eddies over a certain period of time that was the lesser of the eddy lifetime and the transition time. For particles that moved out of the square duct in the streamwise direction, periodic boundary conditions were used to reintroduce them into the computational domain.

Particle and fluid densities were set to $\rho_p = 2500\text{kg/m}^3$ and $\rho_f = 1000\text{kg/m}^3$, respectively, and the kinematic viscosity of fluid was $\nu = 1.004 \times 10^{-6}\text{m}^2/\text{s}$. The particle relaxation time can be calculated as $\tau_p = \rho_p d_p^2 / 18\rho_f \nu$, and the dimensionless particle response

time is defined as the particle Stokes number $St = \tau_p u_\tau^2 / \nu$. Four particle diameters were considered, namely $d_p = 5, 50, 100, \text{ and } 500 \mu\text{m}$. Details of the particle relaxation time, and other relevant parameters, are shown in Table 1. In this study, the particle size was smaller than the corresponding grid size used in the computational domain and at least three time-steps were required for a particle to pass through one fluid control volume unit, hence the particle trajectories were sufficiently resolved.

3. Results and discussion

3.1 Flow field analysis

For the fully developed single-phase flow, Fig. 2 shows a comparison between the present predictions of axial mean velocity profiles along the lower wall bisector ($y=h/2$) and the available experimental data of Melling and Whitelaw (1976) at $Re_b=42\text{k}$, Brundrett and Baines (1964) at $Re_b=83\text{k}$, and Po (1975) at $Re_b=250\text{k}$. It can be seen that the predicted distributions show good agreement with the previous experimental studies of duct flows. In addition, it is found that the mean velocities decrease with the Reynolds number and the distributions tend to be flattened in the central regions of the duct, which is also observed by Gessner and Jones (1965). This may be due to the increasing velocity gradients in the near-wall areas.

Fig. 3 gives the predicted time-averaged secondary flow velocity vectors normalized by the bulk velocity, and corresponding streamwise vorticity contours, in the cross section of the duct at three Reynolds numbers. It can be seen that instantaneously there exists at least two counter-rotating vortices in each corner of the duct, which can be clearly seen in the corresponding vorticity contours. These secondary vortices transfer the streamwise momentum toward the corner regions from the center of the duct, in turn causing the velocity distribution close to the wall to distort and bulge towards the channel corner. In addition, it may also be noted that, with increases in Reynolds number, the time-averaged vorticity distribution tended to become more

uniform and stronger close to the corner regions, which is due to the increased turbulent mixing in the transverse plane. In addition, the core of the secondary vortices also tends to approach the floor and the corner of the duct with increasing Reynolds number. Regarding the effect of Reynolds number on the turbulence statistics, turbulence quantities along the lower wall bisector were studied in previous work (Yao and Fairweather, 2012), where it was found that at lower Reynolds numbers there is more anisotropy in the turbulent normal stresses along the wall bisector, much as is found in channel flows. Furthermore, the normal stresses were found to increase with flow Reynolds number. This is again due to the increased turbulent mixing in the transverse plane with Reynolds number which results in higher instantaneous velocities in the secondary vortices.

The results for the single-phase flow demonstrate that the proposed simulation method is capable of accurately describing the characteristics of flow field in the duct, including the turbulence-driven secondary motions. Based on this, the extension of the simulations to include particle tracking should provide reliable predictions for one-way coupled, particle-laden flows.

3.2 Particle field analysis

Particle resuspension is considered as multiple particles moving away from locations near the duct walls, i.e. the bottom or a sidewall of the duct. If the location of a particle is within 1.5 particle diameters of the wall, the particle is then considered to deposit on the wall and released from the calculation. Multiple particle resuspension is studied statistically based on the resuspension rate as defined above. The resuspended particles have upward (positive) velocities in the x -direction and were monitored in five regions equally spaced in the lower half of the square duct (shown in Fig. 4 (a)). The five regions, from closest to the duct floor to adjacent to the duct's central plane, are labelled "A", "B", "C", "D" and "E". Fig 4(b) shows the velocity vectors of resuspended particle in the monitored regions.

3.2.1 $Re_b = 36.5k$ flow

For the $Re_b = 36.5k$ flow, particle resuspension in the vertical direction was studied for multiple particles, with four sizes 5, 50, 100, and $500\mu m$ considered. The number of particles monitored within the regions noted was sufficient to guarantee the statistical independence of results, which was verified previously by Yao et al. (2009).

Fig. 5 showed the predictions of particle resuspension rate distribution over the five regions in the lower half of the duct at $t^+ = 1972$, where t^+ represents the dimensionless time in wall units. The lift force was not considered here so that the effect of the secondary flows can be investigated. It is apparent from the results that the resuspension rate in the regions closest to the sidewalls is higher than in other regions for all sizes of particles. For $5\mu m$ particles, the resuspension rate is relatively high in the center region. This is mainly due to the effect of the secondary flow that provides an obvious upward motion for particles in the duct center region. Such observations coincide with previous results (Yao and Fairweather, 2010) that particle resuspension does occur near the central plane and the sidewalls. However, for $500\mu m$ particles there is almost no resuspension in the $Re_b = 36.5k$ flow at the indicated time. This is likely due to the fact that large (heavy) particles tend to be dominated by the gravity and quickly deposit on the square duct walls within the indicated time. In addition, to consider particle size effects on resuspension, it is found that with decreasing particle size, particle resuspension appears more prevalent due to particle inertial effects (shown in Fig.5). For the smallest $5\mu m$ particles, these can follow the fluid flow fully due to their low inertia. It is seen that the resuspension of $5\mu m$ particles is more obvious at the sidewalls in comparison with that in the central regions, which indicates that the strength of the secondary flow in the central region is lower than that in the sidewall regions. This will be further considered in Section 3.3.1.

To fully understand the whole particle resuspension process, the extent of particle resuspension with dimensionless time t^+ in the vertical direction was studied, with the results

shown in Fig.6, where t^+ starts from the moment the particles interact with the fluid flow. Fig. 6(a) shows a comparison of mean resuspension rates with increasing t^+ in the five regions noted above for various sizes of particles in the x -direction. It can be seen that for the smallest $5\mu m$ particles, the mean resuspension rate is almost equal to 0.5 and remains stable in all five regions. This means that approximately half of the $5\mu m$ particles are resuspended in the lower half of the duct. For the medium sized particles, at 50 and $100\mu m$, their resuspension rate decreases with time indicating that these particles tend to gradually deposit on the duct floor. For the largest $500\mu m$ particles, the resuspension rate in all five regions remains almost zero from the start of the simulation, indicating that these particles deposit on the duct floor in a short time and are never resuspended. The time-dependent average resuspension rate for different sizes of particles in the x -direction reveals that the smallest particles ($5\mu m$) were most likely to undergo resuspension and reach a statistically dynamic equilibrium state with a constant value of the resuspension rate. As such, this suggests that, for particles of $5\mu m$ diameter or less, the average resuspension rate in all five regions remains constant, and is independent of time. This is mainly due to the fact that the secondary flow in the square duct dominates the motion of small particles. In addition, the secondary flow also causes resuspension of large particles (50 , 100 and $500\mu m$), but its strength in the $Re_b=36.5k$ flow is insufficient to support them in reaching a dynamic equilibrium resuspension state due to the large effect of gravity on them. These results agree with the work of Adams and Fairweather (2011), where the mean displacement of small particles in the vertical direction was found to remain constant. but decrease with time for large particles.

In addition, it was also found that the length of time of particle resuspension is inversely proportional to the particle size. For example, the dimensionless resuspension length of time in region “E” (as shown in Fig.4 (a)) is $41,075$ for $50\mu m$ particles, $27,825$ for $100\mu m$ particles, and $2,650$ for $500\mu m$ particles. These results demonstrate that the turbulence-driven secondary

flow indeed dominates the resuspension process of large particles, although its effect decreases with particle size. Fig. 6(b and c) shows the distribution of the particle mean resuspension rate in the x direction at $t^+=2,650$ and $14,575$. It can be seen that the resuspension rate varies significantly with particle size: for example the $5\mu m$ particles have the highest resuspension rate and the $500\mu m$ particles have the lowest. In addition, the mean resuspension rates for the 50 and $100\mu m$ particles are found to increase with the height in the duct in the x direction. All these results can be further analyzed using the mean particle resuspension velocity normalized by the mean friction velocity in each region, as seen Fig.7.

It is obvious from Fig. 7(a) that the mean resuspension velocity in each region decreases with time for all particles. The smallest $5\mu m$ particles tend to a constant resuspension velocity with time, whilst all other larger particles (50 , 100 and $500\mu m$) tend to deposit on the floor of the duct before reaching a dynamic equilibrium resuspension state. This indicates that the effect of secondary flow on the particles gradually decreases with time due to the balancing effect of gravity, and ultimately becomes stable. Furthermore, it can be seen from Fig. 7(b) that the mean particle resuspension velocity in each region increases with decreasing particle size, corresponding with the variation in the mean resuspension rate (shown in Fig. 6(b)). This is due to the fact that the small particles respond more rapidly to the local flow due to their lower response time, while the response time of larger particles is greater than the characteristic time scale of large-scale vortex structures in this flow, which causes them to respond slowly to the flow. The mean resuspension velocity was also found to increase with height in the duct, as was also found for the resuspension rate (shown in Fig. 6(b)). This implies that the mean strength of the secondary flow in the upper regions of the lower half of the square duct is greater than that in the lower regions.

Fig. 8 shows particle tracks for the considered particle sizes at $t^+=1,325$, $7,780$ and $34,450$ (top to bottom). It is clear that there is no obvious deposition of the $5\mu m$ particles at all given

times, while for the 50, 100 and 500 μm particles, all ultimately deposit on the duct floor with the deposition sequence, in time, being 500 μm < 100 μm < 50 μm . Contrasting these results to those in Fig. 7(a), it can be concluded that particle resuspension has the opposite trend to that of deposition with particle size. According to Yao and Fairweather (2012), gravity most significantly affects particle deposition in the vertical direction. As such, for large particles, gravity plays a key role in their resuspension process, which results in their lower resuspension rates and shorter resuspension times in comparison with small particles.

Overall, the particle resuspension process in the x direction in the $Re_b=36.5k$ flow can be summarized as follows. First, the secondary flow dominates particle resuspension in regions near the center and sidewalls of the square duct, with more resuspension found in the sidewall regions. Second, the mean resuspension rate in the five regions covering the lower half of the square duct increases with decreasing particle size, while the time length of resuspension decreases with particle size. Third, the smallest 5 μm particles are likely to undergo resuspension, with their mean resuspension rate reaching a dynamic equilibrium state in each region at a constant value of 0.5 under the effect of the secondary flow. However, at $Re_b=36.5k$, the secondary flow is insufficient to support the long-term resuspension of larger particles (50, 100 and 500 μm) because all these particles eventually deposit on the duct floor under the effects of gravity effect. Fourth, the mean resuspension velocity in each region decreases with particle size as well as with time. Gravity dominates large particle resuspension, which results not only in a shorter resuspension process but also a lower resuspension rate in comparison with smaller particles.

3.2.2 $Re_b=83k$ flow

For the $Re_b=83k$ flow, the analysis method was the same as that for the $Re_b=36.5k$ flow in the x -direction, with similar conclusions. It was, however, found that particle resuspension profiles in the y -direction over the five regions became more variable than for the $Re_b=36.5k$ flow due

to the higher levels of turbulence. The mean resuspension rate in each region increased with Reynolds number for the 50, 100 and 500 μm particles, and the flow with either the 5 μm or 50 μm particles was able to reach a dynamic equilibrium resuspension state. The constant mean resuspension rate was approximately 0.5, and was independent of time. This is likely due to the greater strength of the secondary flow at the higher Reynolds number, although the resuspension rate of the 100 and 500 μm particles still eventually decreased to zero under the effect of gravity, taking a longer time for resuspension in comparison with that which occurred in $Re_b=36.5k$ flow.

It was also found that the resuspension velocity increased with decreasing particle size because the smaller particles with lower inertia tend to more closely follow the turbulent flow while the larger particles with higher inertia respond less rapidly. Furthermore, the mean velocity in the five regions of the $Re_b=83k$ flow was larger than in the $Re_b=36.5k$ case for all particles, although the velocity difference between different sizes of particles in the $Re_b=83k$ flow was smaller than that in $Re_b=36.5k$ case, which is most likely due to the increased turbulent mixing that occurs with increasing the flow Reynolds number.

Except for the difference as analyzed above, the conclusions obtained for the $Re_b=83k$ flow are generally in line with those for the $Re_b=36.5k$ flow.

3.2.3 $Re_b=250k$ flow

In comparison with the lower Reynolds number flows, turbulence levels are greatly increased in the $Re_b=250k$ flow. The distribution of resuspension rates at $t^+=9,319$ over the five regions in this flow are given in Fig. 9, where the lift force was ignored. It is seen that the particle resuspension is dominant in the central regions and the areas near the sidewalls of the duct. However, the resuspension rate profiles along the y -direction become more variable than those in the lower Reynolds number flows in all five regions and for all sizes of particles. This is due to the fact that the higher instantaneous velocities of the secondary flow have more effect on

the motion of the particles in the y -direction. It is also found that for the $500\mu m$ particles the mean resuspension rate near the sidewalls is higher than in the central regions, which is likely due to the increased strength of the secondary flow that occurs in the duct sidewall regions, as seen in Fig.5.

Using the same analysis as for the cases with lower Reynolds numbers, the time-dependent mean resuspension rates in the five regions are given in Fig. 10. Because the results for the $5\mu m$ particles in this flow were almost the same as those for the $50\mu m$ particles, in analyzing for the effects of Reynolds number on particle resuspension, the case of the $5\mu m$ particles is not considered further. It can be seen from Fig. 10(a) that in this flow the mean resuspension rates of the 50 and $100\mu m$ particles in all regions of the duct are approximately 0.5 , while the resuspension rate for the $500\mu m$ particles decreases to zero, as also occurred in the lower Reynolds number flows ($Re_b=83k$ and $36.5k$), although such resuspension lasted for longer times than in the latter case. As such, it can be concluded that particle resuspension increases with Reynolds number due to the increasing strength of the secondary flow.

In addition, it is worth noting that in this flow ($Re_b=250k$) the mean resuspension rates for all sizes of particles in each region are very similar before $t^+=49k$, but after that the resuspension rate of the $500\mu m$ particles tends to decrease. This is be further verified through the results of Fig.10 (b and c). To analyze this phenomena in more detail, the corresponding mean resuspension velocities normalized by the corresponding friction velocity in the five regions of the duct for each of the considered particles is given in Fig. 11. It can be seen that the mean resuspension velocities in this flow ($Re_b=250k$) are larger than those in the low Reynolds number flows due to the greater turbulence kinetic energy in the flow. In line with the conclusions for the low Reynolds number cases obtained above, the mean resuspension velocity in each region decreases to a constant level, except for the $500\mu m$ particles that eventually deposit on the duct floor due to the effects of gravity. This indicates that the influence of the

secondary flow on particle resuspension gradually tends to a stable state, which leads to a dynamic equilibrium in the resuspension of the 5, 50 and 100 μm particles. It can also be noted that the resuspension velocities of different sizes of particles in each region are very similar before $t^+=49k$, which results in the similar resuspension rates in Fig. 10. This demonstrates that the effect of particle size on particle resuspension declines with flow Reynolds number, which is most likely due to the increased turbulent mixing in the transverse plane. From Fig. 11(b and c), it can be noted that the mean resuspension velocity increases with height in the duct, as for the lower Reynolds number cases, although its effect declines with time.

Table 2 gives a comparison of the average resuspension rate over the whole lower half of the duct for all considered particles in the various Reynolds number flows at the end of the simulations (for $Re_b = 36.5k$ at $t^+=2385$, $Re_b = 83k$ at $t^+=4628$, and $Re_b = 250k$ at $t^+=11951$). It is clear that the average resuspension rate increases with the Reynolds number for all sizes of particles due to the increase of the strength of the secondary flow. The effect of particle size on resuspension is also found to decline gradually with flow Reynolds number. For example, in the $Re_b = 36.5k$ flow, the mean resuspension rate is 0.497 for the 5 μm particles and 0 for the 500 μm particles, while in the $Re_b = 250k$ flow, they are equal to 0.517 for the 5 μm particles and 0.428 for the 500 μm particles. Combined with the previous analysis, it can be concluded that once the particles reach a dynamic equilibrium state, the total resuspension rate is approximately 0.5 regardless of particle size. For example, in the $Re_b = 250k$ flow, the 5, 50 and 100 μm particles are all in a dynamic equilibrium state with stable resuspension rates of 0.517, 0.513 and 0.499, respectively (shown in Fig. 10), with these values independent of time. This can be explained because the number of particles with positive and negative velocities in the vertical direction reach a balance at the dynamic equilibrium condition, which means that the average resuspension rate will be equal to 0.5 in the lower half of the duct.

Particle resuspension in the $Re_b = 250k$ flow can therefore be summarized as follows. The

resuspension rate profiles in the x -direction are more variable than in the lower Reynolds number case for all sizes of particle. Particle resuspension increases with Reynolds number, with the mean resuspension rate of the 5, 50 and $100\mu\text{m}$ particles in the five regions considered remaining constant (at around 0.5), and independent of time. It suggests that all particles reach a dynamic equilibrium state in this flow. The effect of particle size on resuspension decreases with flow Reynolds number, and the mean resuspension velocity in each region also approaches a constant level towards the end of the simulations.

3.3 Mechanism of particle resuspension in turbulent duct flows at various Reynolds numbers

3.3.1 Particle resuspension mechanism

Taking the $Re_b=83k$ case as an example, the particle resuspension mechanism in turbulent duct flows can be explained through Fig. 12 which presents the distribution of particle velocity vectors in the cross-plane of the duct. It is seen that these particles (about 10% of the total number of suspended particles) have relatively high velocities in the x -direction, without this leading to changes in the main trends of the distribution noted earlier. Furthermore, it is found that tracking particles with high velocities in the x -direction results in their locations appearing mainly in two regions, one near the sidewalls and the other at the center of the duct, which causes the higher resuspension rates in these regions noted in Figs. 5 and 9. It can also be noted that the distribution of particles near the sidewall regions is denser than that in the central region, which is most likely due to spatial differences in the intensity of secondary flow. This explains the relatively high resuspension rates in regions close to the sidewalls noted in Section 3.2.1. In addition, it is also observed that the number of particles with high velocities increases with the height in the duct, which causes high total mean particle resuspension velocities in the upper regions, as seen in Figs. 7(b) and 11(b), as well as high resuspension rates in these regions.

3.3.2 Dynamic analysis

To further understand the mechanisms leading to particle resuspension in duct flows, the dynamic force acting on particles in the resuspended state was analyzed. By comparing the resuspension rate in the various Reynolds number flows, it is found that the mean resuspension rate in each region within the duct for the $5\mu\text{m}$ particles in the $Re_b=36.5k$ flow, for the 5 and $50\mu\text{m}$ particles in the $Re_b = 83k$ flow, and for the 5, 50 and $100\mu\text{m}$ particles in the $Re_b = 250k$ flow, has a value of approximately 0.5 in all cases, with this value independent of time. This result suggests that these particles were in a statistically steady state in terms of the forces acting upon them. This is confirmed by the results given in Fig. 13(a to d), which gives plots of the resultant force acting on the particles in their statistically steady, resuspended state, normalized by $\rho_f \nu^2$ (where ν is the fluid kinematic viscosity). It is observed that the mean total resultant force acting on these particles tends to a stable state with increasing time in all five regions. This can also be concluded from the results of Fig. 7(a) and Fig. 11(a), where the slope of the resuspension velocity remains constant after $t^+=20k$ and $t^+=50k$, respectively. It is suggested that particles in the dynamic equilibrium resuspension state have a constant acceleration in the x -direction. In contrast, the resultant force acting on other particles finally leads them to deposit on the duct floor, which fluctuates significantly with time during the period of the resuspension.

The absolute mean forces, including the drag force and lift force, acting on all sizes of particles in the resuspension state over the whole lower half of the duct at various Reynolds numbers are given in Table 3. It can be seen that both the drag and lift force increase with particle size, which agrees well with the findings of Sommerfeld and Kussin (2003). For the smallest $5\mu\text{m}$ particles, the lift force is at least orders of two magnitude less than the drag force for all Reynolds number flows. As such, it is the drag force that dominates small particle resuspension in the x -direction. However, with particle size increasing as well as inertia, the lift

force gradually increases and becomes significant in determining particle resuspension. For instance, in the $Re_b = 36.5k$ flow for the $100\mu m$ particles the mean lift force is equal to $5.38 \times 10^{-9}N$, which is larger than the drag force of $2.21 \times 10^{-9}N$. Such conclusions are in line with the results of Yao and Fairweather (2010).

Fig. 14 shows the mean drag force and lift force, nondimensionalized by $\rho_f v^2$, acting on the resuspended particles versus time at the various Reynolds numbers considered. It is found that the drag force in all Reynolds number flows gradually decrease with increasing time, and this trend is more obvious for larger particles. This is mainly due to the corresponding decrease in the particle velocity, as seen in Fig.7 (a) and Fig.11 (a), which results in a decrease in the slip velocity between the fluid and the particle, as observed in the work of Yao and Fairweather (2010). It is suggested that the effect of the drag force on particle resuspension gradually decreases with time, but that this decrease declines with increasing Reynolds number due to the increasing transverse mixing in the high Reynolds number flows. Conversely, the lift force increases with time over all regions in all flows. This is likely due to the fact that the lift force is not only related to the slip velocity but also to the fluid streamwise velocity gradient which is dependent on the Reynolds number. With increasing time, under the effect of gravity, more and more particles tend to approach the duct floor, where high fluid velocity gradients dominate and thereby increase the lift force. Furthermore, the boundary layer becomes thinner with the increase in Reynolds number and the effect of the velocity gradient on the lift force tends to be reduced in the broad regions away from the wall. In addition, it can also be seen that the drag force increases with the height in the duct at all Reynolds numbers, which also relates to the similar tendency in the resuspension velocity, as seen in Fig.7 (b) and Fig.11 (b). This implies that there is a large difference in the slip velocity between the particle and the fluid in the upper and lower regions of the lower half of the duct, with such differences declining with Reynolds number due to the stronger transverse mixing in the high Reynolds number flows. In contrast

to the drag force, the lift force acts inversely with the height in the duct in all flows, which indicates that the streamwise fluid velocity gradient dominates the lift force in the lower regions of the duct. This variation with height decreases with increasing Reynolds number, as shown in Fig.14 (e), where the drag and lift force in all five regions tend to be very similar. This finding indicates that the drag force dominates particle resuspension in the upper region of the lower half of the duct, whilst the lift force mainly dominates particle resuspension in the lower region, especially for the low Reynolds number flows. The effect of height in the high Reynolds number flow is not so obvious as in the lower Reynolds number flows due to the strong turbulent mixing in the plane of the duct cross-section, which results in relatively low velocity gradients in the x -direction and causes the small difference between the of drag and lift forces over the five regions.

4. Conclusions

Particle resuspension in turbulent duct flows at three Reynolds numbers ($Re_b=36.5k$, $83k$ and $250k$) has been investigated using large eddy simulation coupled with the Lagrangian particle tracking technique. Four particle sizes (5 , 50 , 100 and $500\mu m$) have been considered in studying particle resuspension in the vertical, x -direction. The conclusions can be summarized as follows.

In the same Reynolds number flow, particle resuspension mainly occurs in regions close to the center and the sidewalls of the duct. The mean resuspension rate in these regions decreases with particle size due to the effects of gravity. Smaller particles are more easily resuspended and achieve a statistically stable resuspension rate. Furthermore, for particles deposited on the duct floor, it is found that the smaller particles are able to remain a longer time in resuspension in comparison with other particles. Under the effect of the secondary flow, the mean resuspension velocity gradually decreases to a stable value with time. The mean resuspension

velocity increases with height in the duct, which implies that the secondary flow strength in the upper regions of the lower half of the duct is stronger than in the lower regions, resulting in a fairly low resuspension rate there.

For various Reynolds number flows, the particle resuspension rate and resuspension velocity increase with the Reynolds number for all sizes of particles. The resuspension rate profiles in the y -direction over the five regions considered in the lower half of the duct appear more variable with increasing Reynolds number. For the same size of particles, they more readily reach a steady resuspended state, or remain resuspended for a longer time, with increasing flow Reynolds number. The effect of particle size on the resuspension rate gradually declines with the Reynolds number. Once the strength of the secondary flow is able to support a steady particle resuspension rate, the overall mean resuspension rate is close to 0.5, regardless of particle size and Reynolds number.

A dynamic analysis for the resuspended particles shows that both the drag force and lift force acting on the particles increase with particle size. The drag force mainly dominates resuspension for small particles whilst the lift force gradually increases to be a major factor influencing particle resuspension with increasing particle size. For the low Reynolds number flow, the effect of drag force on resuspension decreases with time, but that of the lift force increasing. In addition, the drag force decreases with decreasing height in the duct, whilst the lift force increases with it for all Reynolds number flows, which indicates that the lift force mainly dominates particle behavior in the lower regions of the duct whilst the drag force mainly dominates in the upper regions. However, such effects of height on the particles are not so obvious in the high Reynolds number flows.

In this work, due to the low particle concentrations considered, used to decrease computation times, the effect of particles on the flow have been ignored. Extension to cover flows in which such coupling occurs should be considered further for increased particle concentrations. In

regards to two-way coupling, some effects in fully developed turbulent flows might be expected, as following. First, particles smaller than the dissipative length scale reduce turbulence levels and Reynolds stresses, whereas larger particles increase them. The particle size has an opposite effect on the streamwise mean velocities, i.e. smaller particles increase the mean velocities, while larger particles decrease them. As the settling velocity of the particles is increased, turbulence levels and Reynolds stresses are also increased (Pan and Banerjee, 1996, 1997). Second, the nature of turbulence modification depends on the initial velocity and the distribution of heavy solid particles in the flow domain, and the temporal radial migration of particles towards the wall (Rani and Vanka, 2000). Third, two-way coupling reduces the preferential concentration of particles near the wall, whilst the particles attenuate the mean streamwise velocities and fluid turbulence levels (Portela et al. 1999). As such, particle size, density and concentration will all affect the flow turbulence and vice versa through two-way coupling.

Acknowledgements

This work was supported by the National Natural Science Foundation of China (Grant Nos. 51776225; 51376153; 51406235), the 111 project and the Science Foundation of the China University of Petroleum, Beijing (Grant No. C201602). The authors would also like to express their gratitude to Prof W.P. Jones for providing the BOFFIN LES code and for many helpful discussions on its use.

REFERENCE

Adams, J., Fairweather, M., Yao, J., 2011. Modelling and simulation of particle re-suspension in a turbulent square duct flow. *Comput. Chem. Eng.* 35, 893-900.

Afkhami, M., Hassanpour, A., Fairweather, M., Njobuenwu, D. O., 2014. Reynolds number effects on particle agglomeration in turbulent channel flow. *Computer-Aided Chemical Engineering*. 33, 967-972.

Afkhami, M., Hassanpour, A., Fairweather, M., Njobuenwu, D.O., 2015. Fully coupled LES-DEM of particle interaction and agglomeration in a turbulent channel flow. *Comput. Chem. Eng.* 78,24-38.

Armenio, V., Fiorotto, V., 2001. The importance of the forces acting on particles in turbulent flows. *Phys. Fluids* 13, 2437.

Barth, T., Preuss, J., Muller, G., Hampel, U., 2014. Single particle resuspension experiments in turbulent channel flows. *J. Aerosol Sci.* 71, 40-51.

Barth, T., Lecrivain, G., Jayaraju, S. T., Hamel, U., 2015. Particle deposition and resuspension in gas-cooled reactors—Activity overview of the two European research projects THINS and ARCHER. *Nucl. Eng. Des.* 290,127-134.

Brundrett, E., Baines, W. D., 1964. The production and diffusion of vorticity in duct flow. *J. Fluid Mech.* 19, 375.

Chen, Q. C., Xu, J. L., Sun, D. L., Cao, Z., Xie, J., Xing, F., 2013. Numerical simulation of the modulated flow pattern for vertical upflows by the phase separation concept. *Int. J. Multiphase Flow*, 56, 105-118.

Di Mare, F., 2002. Large Eddy Simulation of Reacting and Non-Reacting Flows in Complex Geometries. Ph.D. Thesis. Department of Mechanical Engineering, Imperial College London.

Di Mare, F., Jones, W. P., 2003. LES of turbulent flow past a swept fence. *Int. J. Heat Fluid Flow* 24,606–615.

Elghobashi, S., 1994. On predicting particle-laden turbulent flows, *Appl. Sci. Res.* 52, 309–329.

Fairweather, M., Yao, J., 2009. Mechanisms of particle dispersion in a turbulent, square duct flow. *AIChE J.* 55, 1667-1679.

Fan, J. R., Yao, J., Cen, K. F., 2002. Antierosion in a 90° bend by particle impaction, *AIChE J.* 48, 1401.

Fu, S. C., Chao, Y. H., So, R. M. C., Leung, W. T., 2013. Particle resuspension in a wall-bounded turbulent Flow. *J. Fluids Eng.* 135, 041301.

Gavrillakis, S., 1992. Numerical simulation of low-Reynolds-number flow through a straight square duct, *J. Fluid Mech.* 244, 101.

Germano, M., 1992. Turbulence, the filtering approach. *J. Fluid Mech.* 238,325.

Germano, M., Piomelli, U., Moin, P., Cabot, W., 1991. A dynamic sub-grid scale eddy viscosity model, *Phys. Fluids A* 3, 1760.

Gessner, F. B., Jones, J. B., 1965. On some aspects of fully-developed turbulent flow in rectangular channels. *J. Fluid Mech.* 23, 689-713.

Gessner, F. B., Po, J. K., Emery, A. F., 1979. *Turbulent Shear Flows* 1, 119.

Huser, A., Biringen, S., 2006. Direct numerical simulation of turbulent flow in a square duct. *J. Fluid Mech.*, 257, 65-95.

Jones Jr, O., 1976. An improvement in the calculation of turbulent friction in rectangular ducts. *J. Fluid Eng.-T. ASME* 98, 173.

Jones, W. P., Wille, M., 1996. Large eddy simulation of a plane jet in a cross flow. *Int. J. Heat Fluid Flow* 17,296–306.

Launder, B. E., Ying, W. M. 1972. Secondary flows in ducts of square cross-section. *J. Fluid Mech.* 54, 289.

Li, D., Wei, A.Y., Luo, K., Fan J. R., 2016. Direct numerical simulation of a particle-laden flow in a flat plate boundary layer, *Int. J. Multiphase Flow*, 79, 124-143.

Lilly, D. K., 1967. The representation of small scale turbulence in numerical simulation experiments, in *Proceedings of the IBM Scientific Computing Symposium on Environmental Sciences*, edited by H. H. Goldstine (IBM, Yorktown Heights), 195–210.

- Madabhushi, R. K., Vanka, S. P., 1991. Large eddy simulation of turbulence driven secondary flow in a square duct. *Phys. Fluids A* 3, 2734.
- di Mare, L., Jones, W.P., 2003. LES of turbulent flow past a swept fence. *Int. J. Heat Fluid Flow* 24, 606.
- Mei, P., 1992. An approximate expression for the shear lift force on a spherical particle at finite Reynolds number, *Int. J. Multiphase Flow* 18, 145.
- Melling, A., Whitelaw, J.H. 1976. Turbulent flow in a rectangular duct. *J. Fluid Mech.* 78, 289-315.
- Middletich, B., 1981. Environmental effects of offshore oil production. Technical Report. Plenum, New York, NY.
- Nicholson, K. W., 1988. A review of particle resuspension. *Atmos. Environ.* 22, 2639.
- Pan, Y., Banerjee, S., 1996. Numerical simulation of particle interactions with wall turbulence, *Phys. Fluids*, 8, 2733– 2755.
- Pan, Y., Banerjee, S., 1997. Numerical investigation of the effects of large particles on wall-turbulence, *Phys. Fluids*, 9, 3786– 3807.
- Pinelli, A., Uhlmann, M., Sekimoto, A., Kawahara, G., 2010. Reynolds number dependence of mean flow structure in square duct turbulence, *J. Fluid Mech.*, 644, 107-122.
- Piomelli, U., Liu, J., 1995. LES of rotating channel flow using a localized dynamic model. *Phys. Fluids* 7, 839.
- Po, J.K., 1975. Developing Turbulent Flow in the Entrance Region of a Square Duct. MS Thesis. Department of Mechanical Engineering, University of Washington.
- Portela, L.M., Oliemans, R.V.A., Nieuwstadt, F.T.M., 1999. Numerical simulation of particle-laden channel flows with two-way coupling, 3rd ASME/JSME Joint Fluids Engineering Conference
- Porte-Agel, F., Meneveau, C., Parlange, M., 2000. A scale-dependent dynamic model for large-

eddy simulation: Application to a neutral atmospheric boundary layer. *J. Fluid Mech.* 415, 261.

Rani, S.L., Vanka, S.P., 2000. Numerical simulation of two-way coupling effects in a particle-laden turbulent pipe flow, ASME Fluids Engineering Summer Conference.

Robinson, S. K., 1991. Coherent motions in the turbulent boundary layer. *Annu. Rev. Fluid Mech.* 23, 601.

Rouson, D. W. I., Eaton, J. K., 2001, On the preferential concentration of solid particles in turbulent channel flow, *J. Fluid Mech.* 428, 149–169

Saffman, P. G., 1965. The lift on a small sphere in a shear flow. *J. Fluid Mech.* 22, 385.

Saffman, P. G., 1968. Corrigendum to ‘The lift on a small sphere in a slow shear flow, *J. Fluid Mech.* 31, 624.

Sehmel, G.A., 1980. Particle resuspension: A review. *Environ. Int.* 4, 107.

Sharma, G., Phares, D. J., 2006. Turbulent transport of particles in a straight square duct. *Int. J. Multiphase Flow* 32, 823-837.

Smagorinsky, J., 1963. General circulation experiments with the primitive equations. *Mon. Weather Rev.* 91, 99.

Soepryan, F.B., Cremaschi, S., McLaury, B.S., Sarica, C., Subramani, H.J., Kouba, G.E., Gao, H., 2016. Threshold velocity to initiate particle motion in horizontal and near-horizontal conduits. *Powder Technol.* 292, 272–289.

Sommerfeld, M., Kussin, J., 2003. Analysis of collision effects for turbulent gas-particle flow in a horizontal channel. Part II. Integral properties and validation. *Int. J. Multiphase Flow* 29, 701-718.

Squires, K. D., Eaton, J. K., 1991. Measurements of particle dispersion obtained from direct numerical simulations of isotropic turbulence, *J. Fluid Mech.* 226, 1 –35.

Wang, Q., Squires, K.D., 1996. Large eddy simulation of particle deposition in a vertical turbulent channel flow, *Int. J. Multiph. Flow* 22, 667– 683.

Wille, M.,1997. Large Eddy Simulation of Jets in Cross Flows .Ph.D. Thesis. Department of Chemical Engineering, Imperial College of Science, Technology and Medicine, London.

Winkler, C.M., Rani, S. L., Vanka, S.P.,2004. Preferential concentration of particles in a fully developed turbulent square duct flow. *Int. J. Multiphase Flow* 30, 27-50.

Winkler C M, Rani S L., 2009. Relative importance of the lift force on heavy particles due to turbulence driven secondary flows. *Powder Technology*, 190, 310-318.

Yao, J., Fairweather, M., 2010. Inertial particle resuspension in a turbulent, square duct flow. *Phys. Fluids* 22, 107-210.

Yao, J., Fairweather, M., 2012. Particle deposition in turbulent duct flows. *Chem. Eng. Sci.* 84, 781–800.

Yao, J., Zhang, Y., Wang, C.H., Matsusaka, S., Masuda, H., 2004. Electrostatics of the granular flow in a pneumatic conveying system. *Ind. Eng. Chem. Res.* 43, 7181.

Yao, J., Zhang, Y., Wang, C.H., Liang, Y.C., 2006. On the electrostatic equilibrium of granular flow in pneumatic conveying systems. *AIChE J.* 52, 3775.

Yao, J., Zhao, Y. L., Fairweather, M., 2015. Numerical simulation of turbulent flow through a straight square duct. *Appl. Therm. Eng.* 91, 800-811.

Yao, J., Zhao, Y. L., Hu, G. L., Fan, J. R., Cen, K. F., 2009. Numerical simulation of particle dispersion in the wake of a circular cylinder. *Aerosol Sci. Tech.* 43, 174–187.

Zeng L, Najjar F, Balachandar S, et al. Forces on a finite-sized particle located close to a wall in a linear shear flow[J]. *Physics of Fluids*, 2009, 21(3):1.

Zhang, H., Trias, F.X., Gorobets A, Oliva, A., Yang, D. M., Tan, Y. G., Sheng, Y., 2015. Effect of collisions on the particle behavior in a turbulent square duct flow. *Powder Tech.* 269, 320-336.

Zhang J, Li A. CFD simulation of particle deposition in a horizontal turbulent duct flow[J]. *Chemical Engineering Research & Design*, 2008, 86(1):95-106.

Zhang, W., Xu, J. L., Liu, G. H., 2008. Multi-channel effect of condensation flow in a micro triple-channel condenser. *Int. J. Multiphase Flow* 34, 1175-1184.

Table 1 Parameters relevant to the simulations of particle resuspension

$d_p(\mu m)$	$Re_b = 36.5k$		$Re_b = 83k$		$Re_b = 250k$		Gravity(N)	Buoyancy(N)
	d_p^+	$St(\tau_p^+)$	d_p^+	$St(\tau_p^+)$	d_p^+	$St(\tau_p^+)$		
5	0.25	0.01	0.48	0.03	1.32	0.24	1.50×10^{-12}	6.01×10^{-13}
50	2.49	0.86	4.83	3.23	13.19	24.15	1.50×10^{-9}	6.01×10^{-10}
100	4.98	3.44	9.65	12.93	26.38	96.62	1.20×10^{-8}	4.81×10^{-9}
500	24.88	85.94	48.25	323.34	131.88	2415.42	1.50×10^{-6}	6.01×10^{-7}

Table 2 Average resuspension rate over the low half of duct for different Reynolds number flows at given time

$d_p(\mu m)$	$Re_b = 36.5k(t^+=2385)$	$83k(t^+=4628)$	$250k(t^+=11951)$
5	0.497	0.515	0.517
50	0.385	0.490	0.513
100	0.286	0.467	0.499
500	0	0.226	0.428

Table 3 Absolute mean forces on resuspended particle in the vertical direction at given time for different Reynolds number case

Re $d_p(\mu m)$	$36k(t^+=2385)$		$83k(t^+=4628)$		$250k(t^+=11951)$	
	Drag (N)	Lift (N)	Drag (N)	Lift (N)	Drag (N)	Lift (N)
5	3.69×10^{-12}	1.06×10^{-14}	2.72×10^{-11}	4.59×10^{-15}	7.20×10^{-10}	3.27×10^{-15}
50	5.18×10^{-10}	4.40×10^{-10}	9.29×10^{-10}	2.80×10^{-10}	5.82×10^{-10}	1.26×10^{-9}
100	2.21×10^{-9}	5.38×10^{-9}	3.86×10^{-9}	4.09×10^{-9}	2.44×10^{-9}	1.77×10^{-8}
500	3.79×10^{-8}	8.27×10^{-7}	9.35×10^{-8}	8.19×10^{-7}	5.39×10^{-7}	1.96×10^{-6}

Figure 1

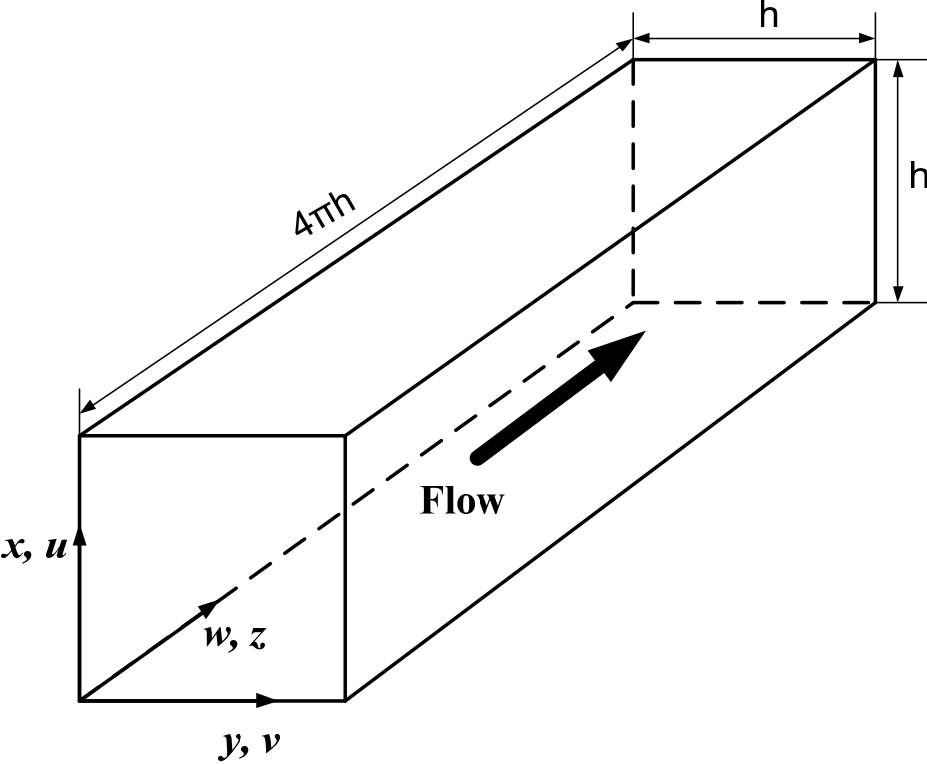


Fig 1 Schematic of the duct geometry

Figure 2

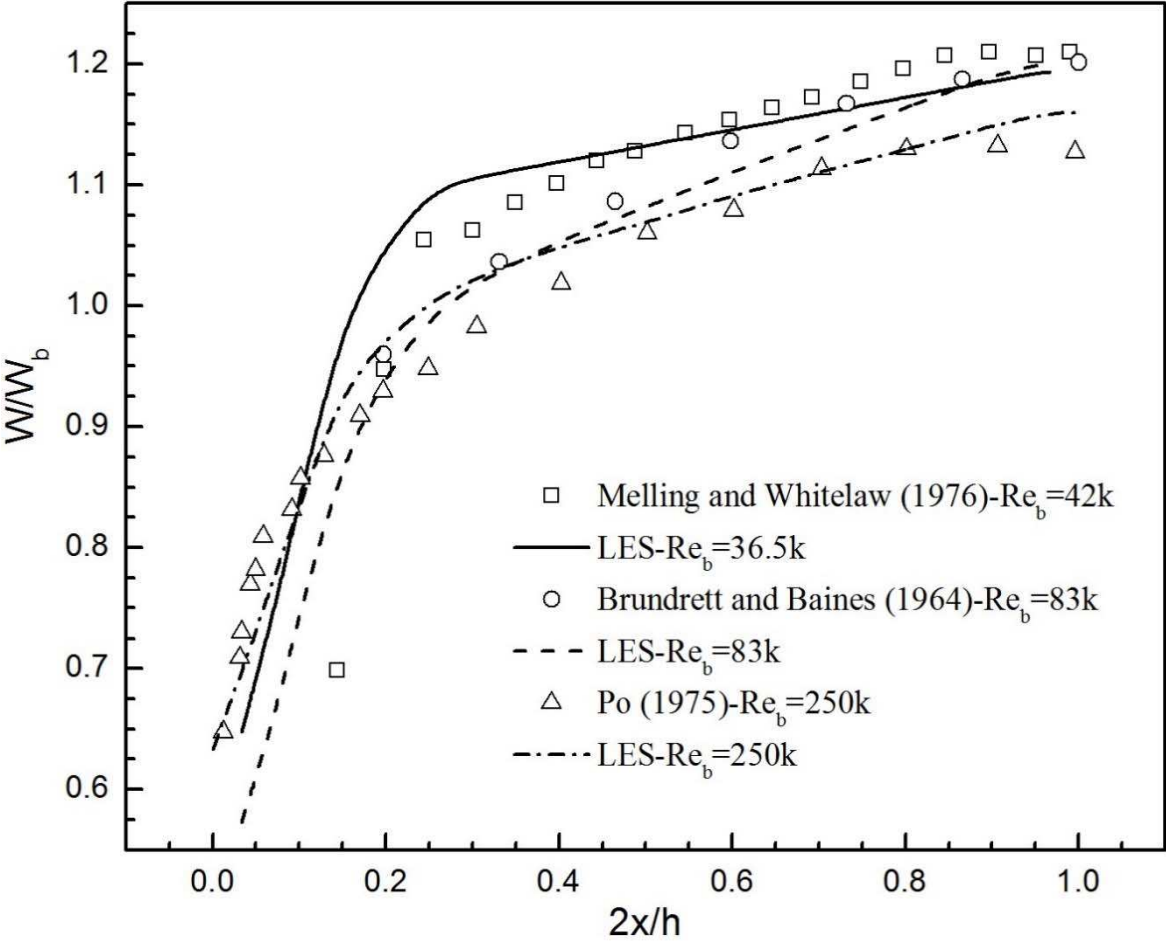


Fig. 2 Mean streamwise velocities along the lower wall bisector at different Reynolds numbers

Figure 3

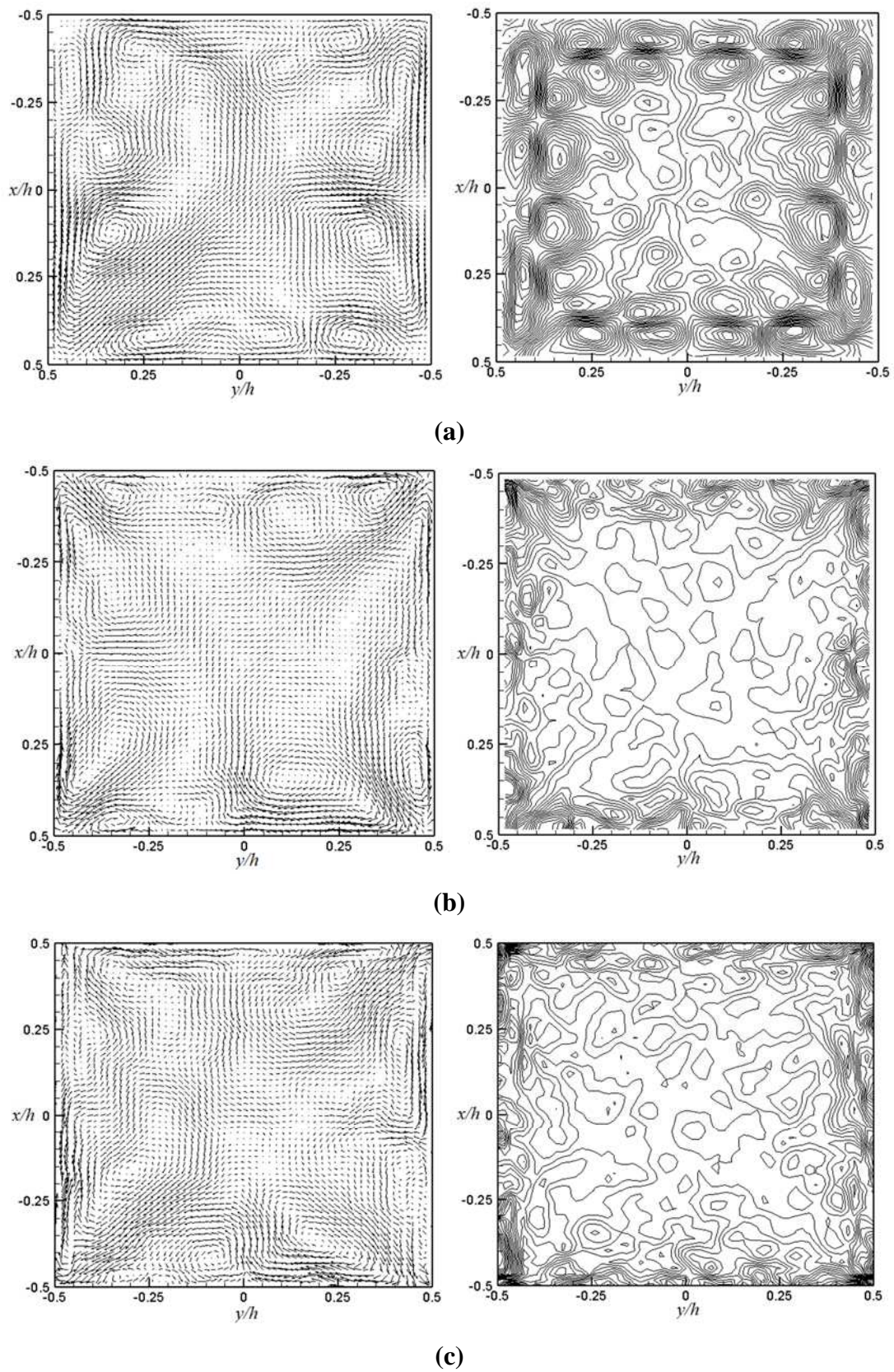
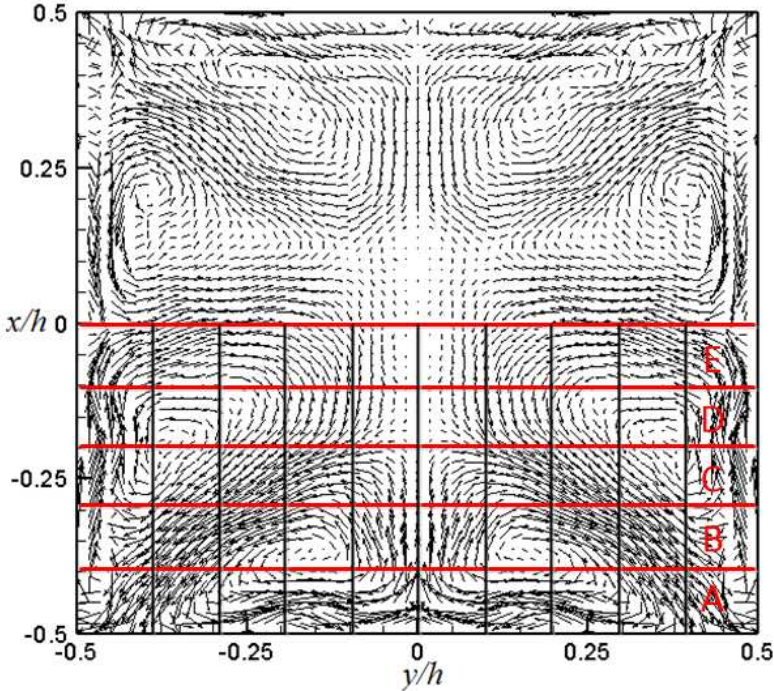
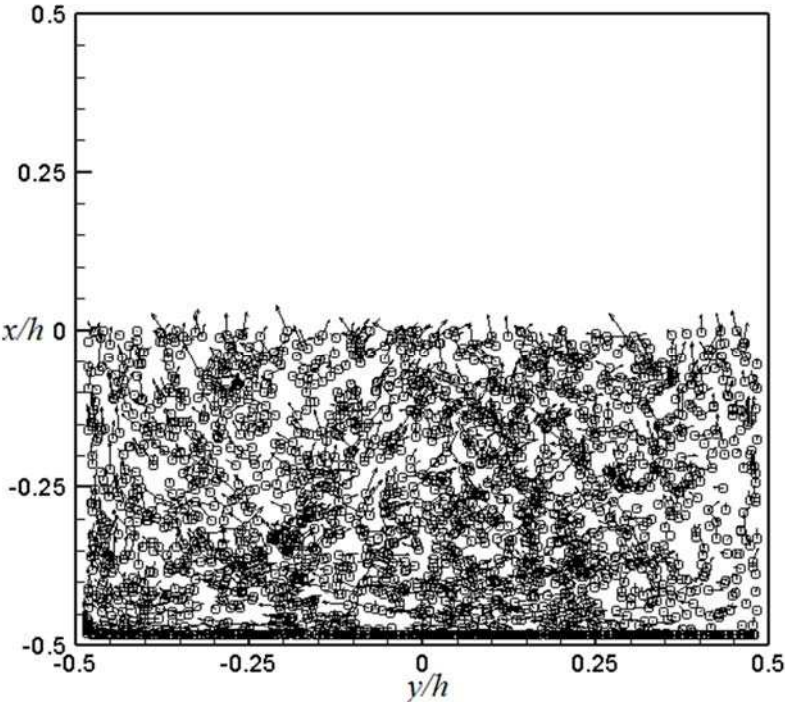


Fig. 3 Time-averaged secondary flows and corresponding streamwise vorticity contours in the whole square duct at $Re_b =$ (a) $36k$; (b) $83k$; (c) $250k$.

Figure 4



(a)



(b)

Fig. 4 (a) Secondary flow in the square duct with grids net for calculating particle resuspension; (b) velocity vectors of particle resuspension in the low half of the square duct.

Figure 5

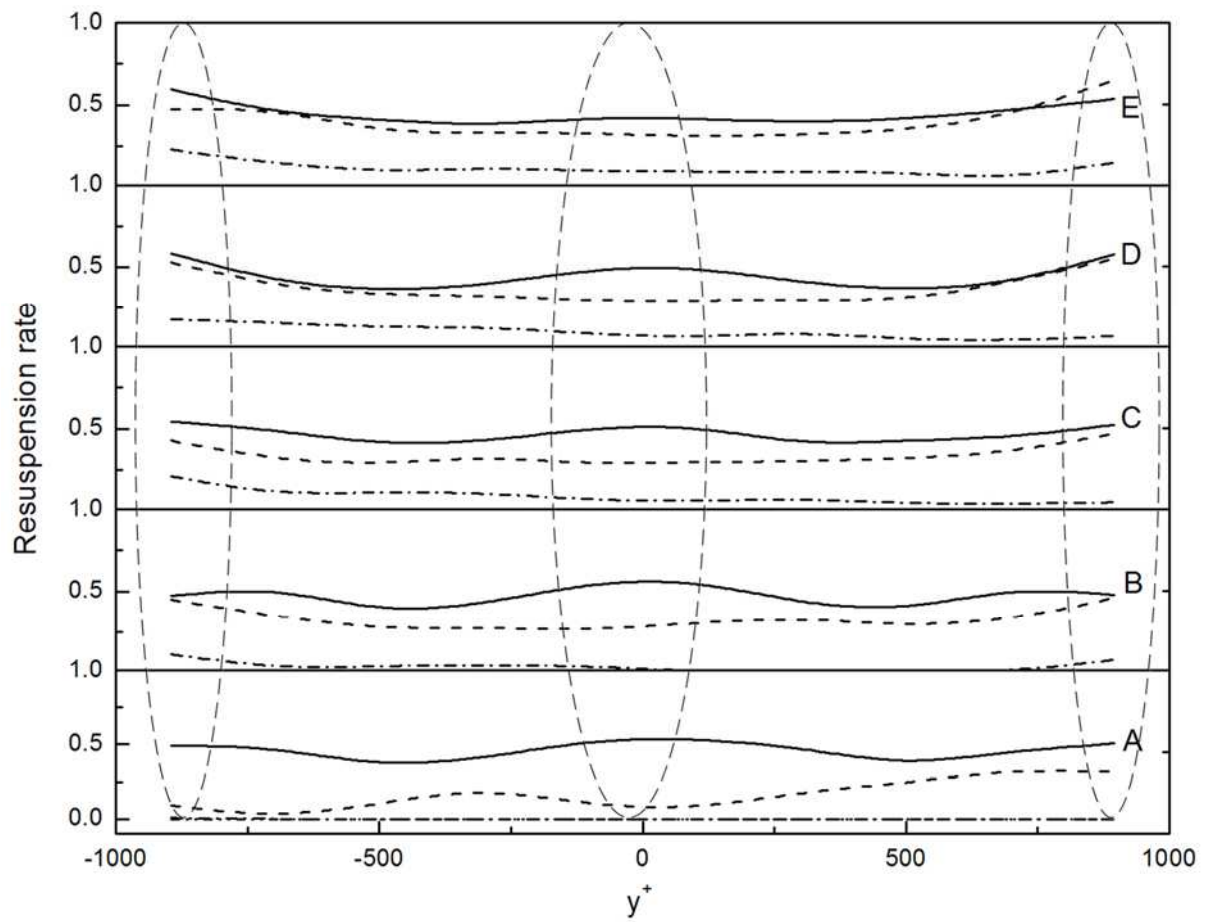
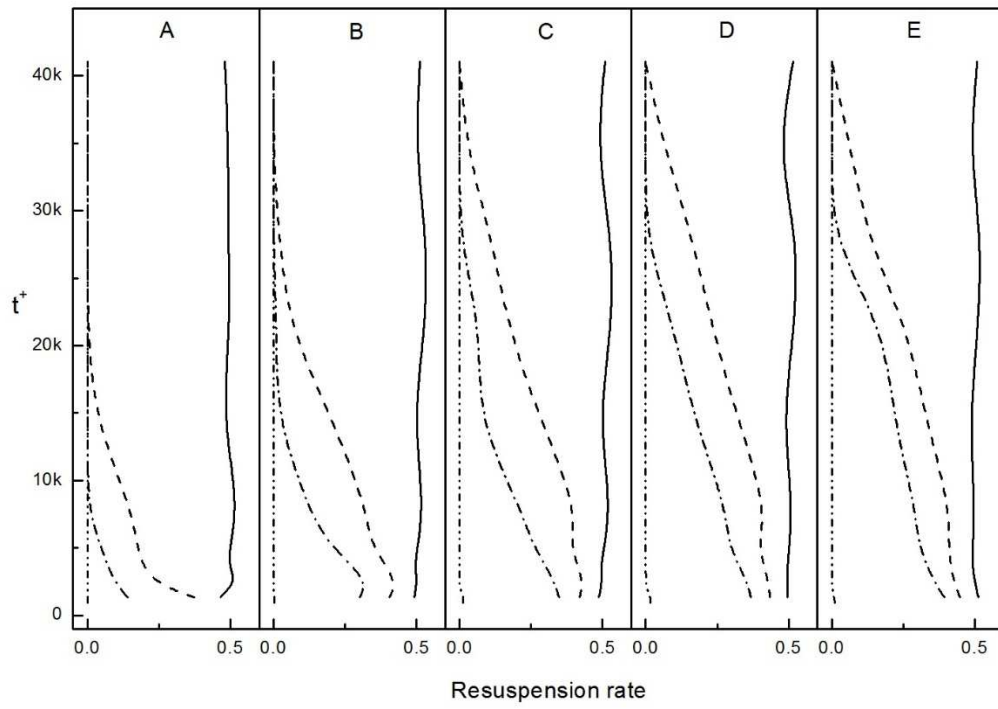
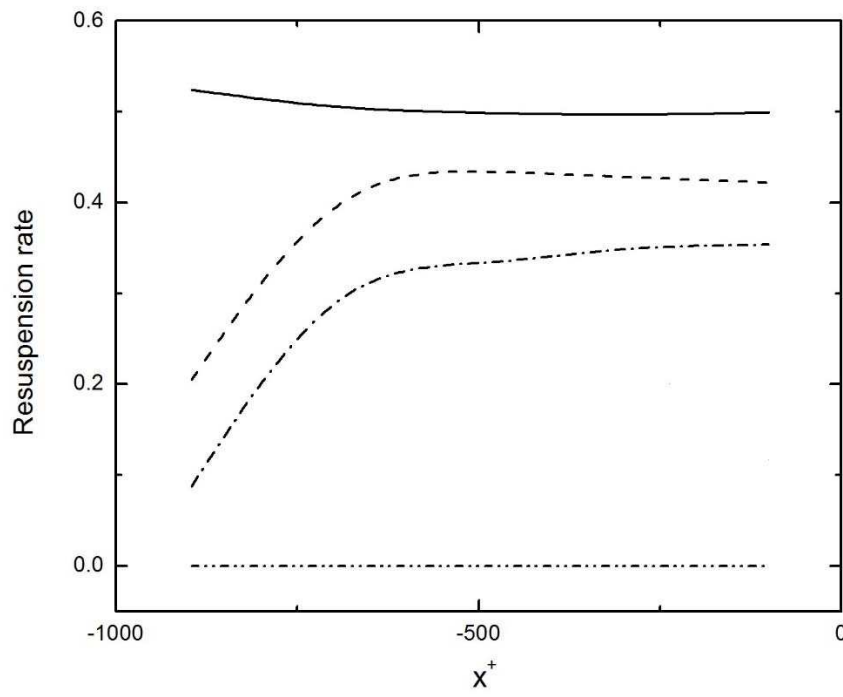


Fig. 5 Particle resuspension rate distribution for 5,50,100,500 μm particles at $t^+=1972$ (no lift) ($Re_b=36k$, — 5 μm , - - - 50 μm , - · - · - 100 μm , - - - - - 500 μm particles)

Figure 6



(a)



(b)

Figure 6 (continued)

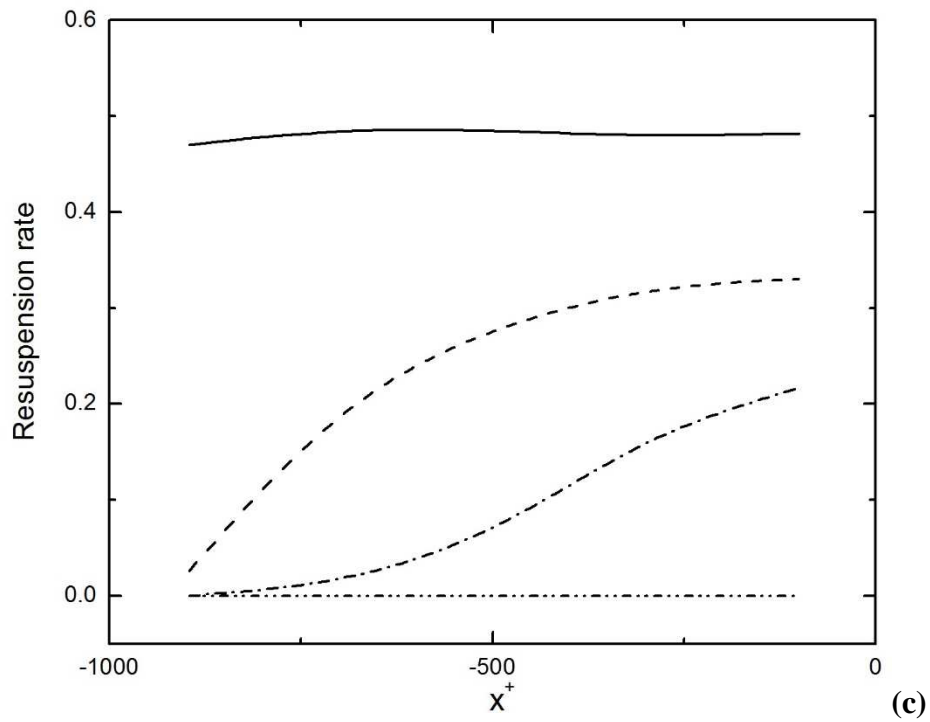
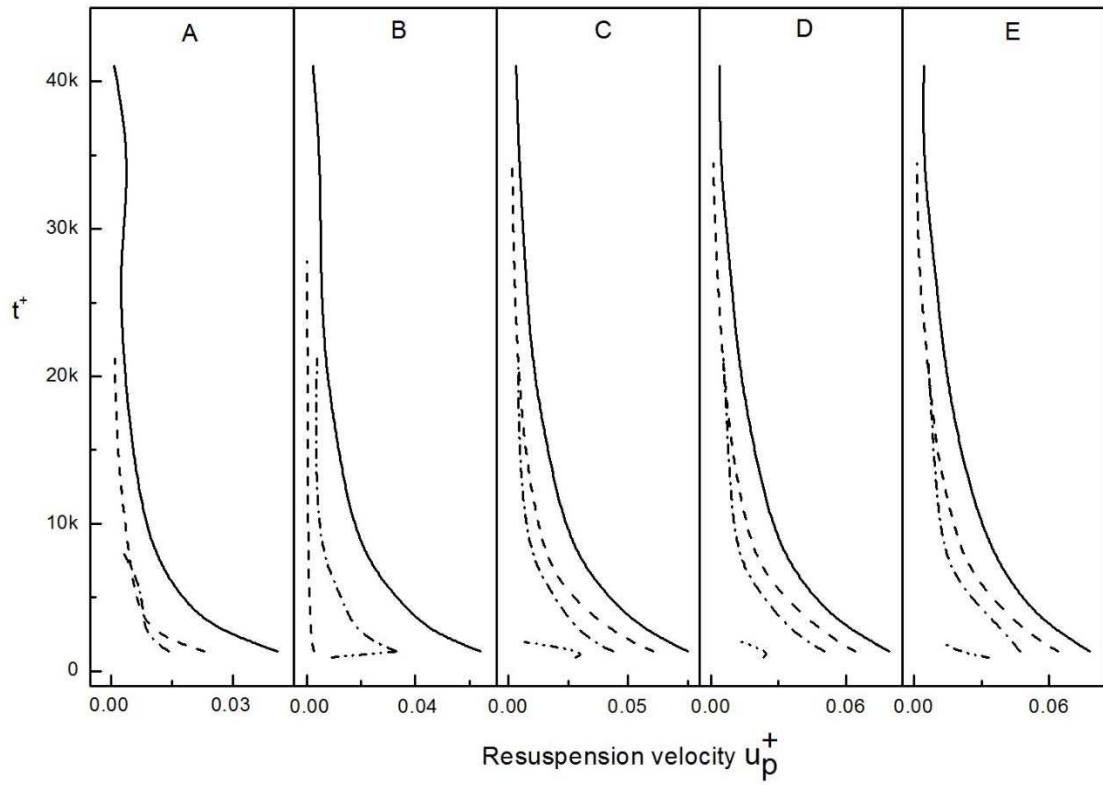
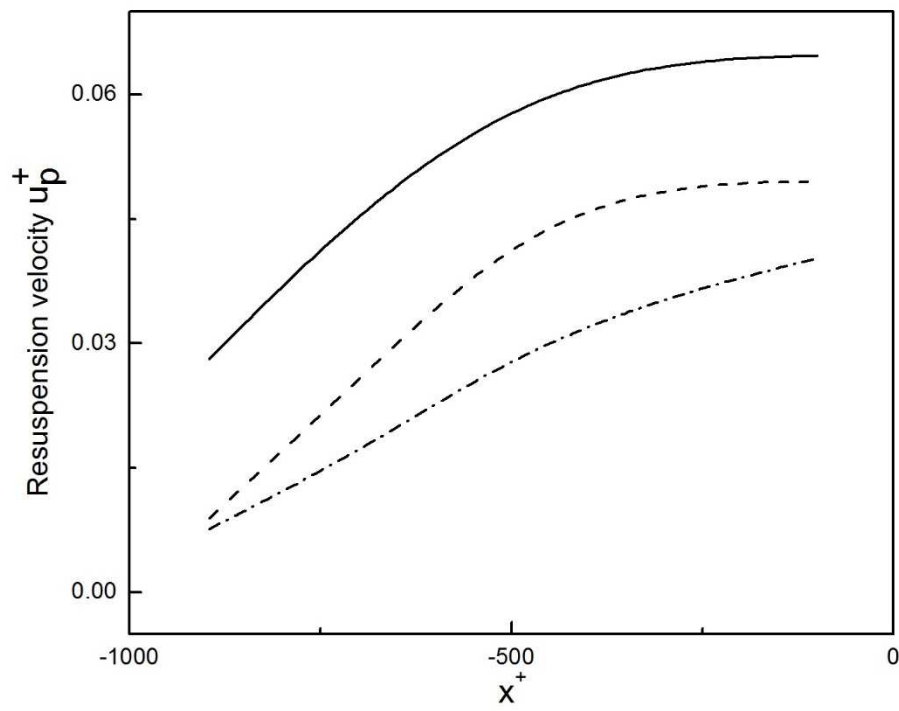


Fig. 6 The mean resuspension rates (a) in five regions with time development; at the x direction (b) at $t^+=1972$, (c) $t^+=14575$ for 5 to $500\mu\text{m}$ particles in the low half of the square duct ($Re_b=36k$,
————— $5\mu\text{m}$, - - - - - $50\mu\text{m}$, - · - · - · $100\mu\text{m}$, - · · - · · $500\mu\text{m}$ particles)

Figure 7



(a)



(b)

Figure 7 (continued)

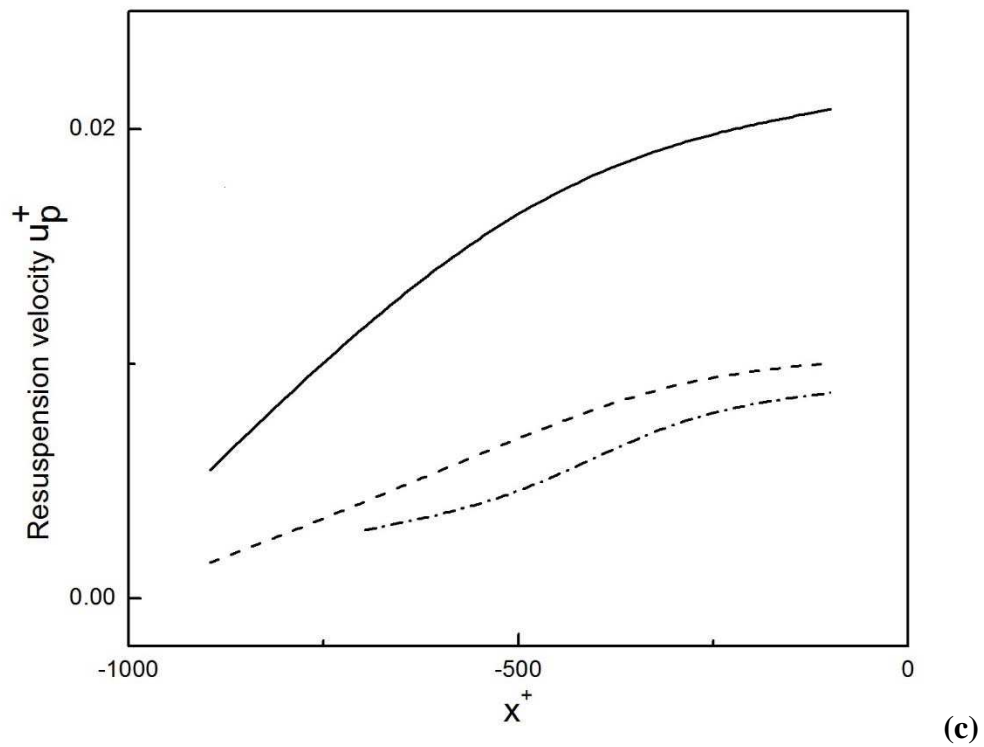
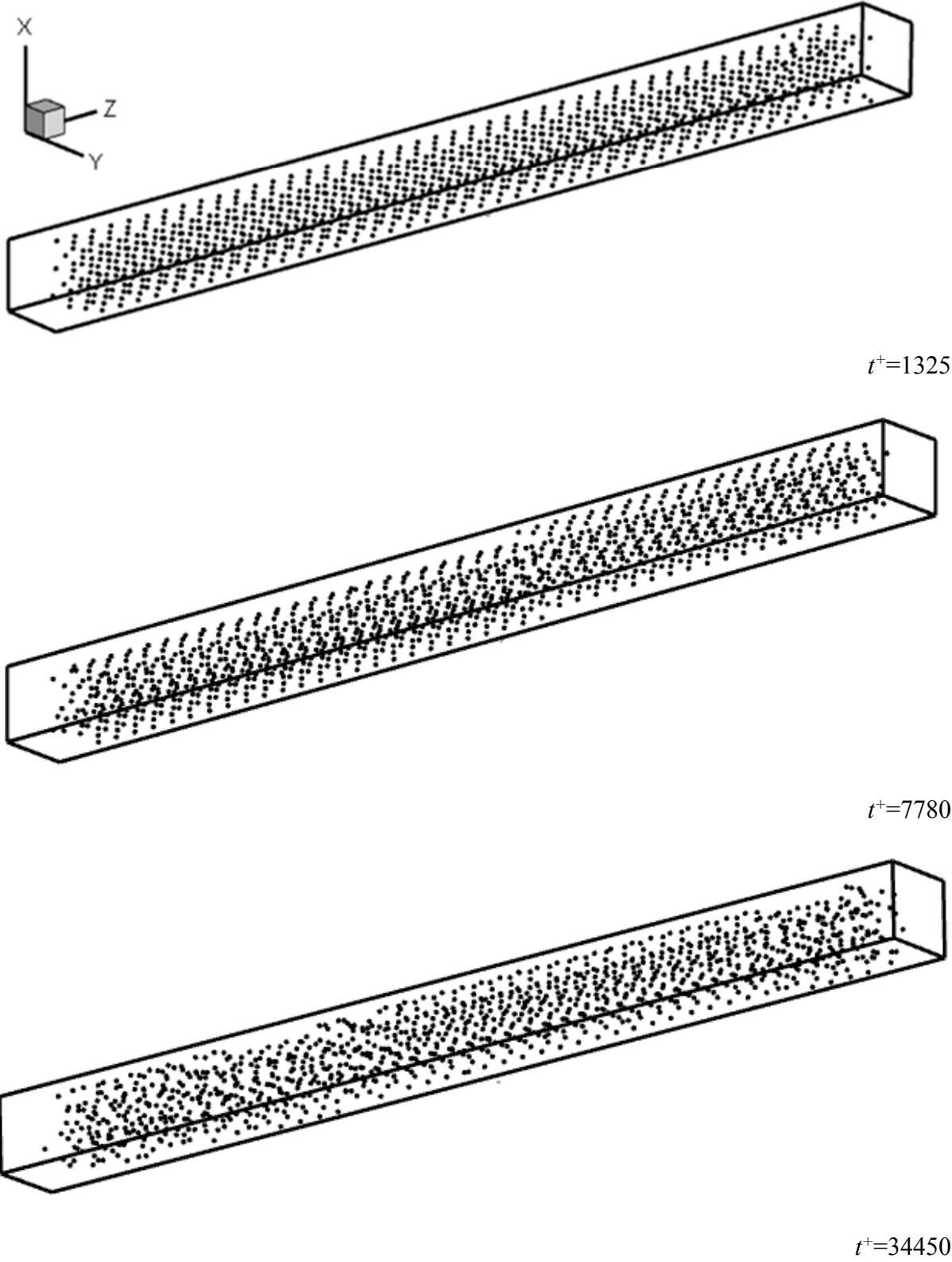


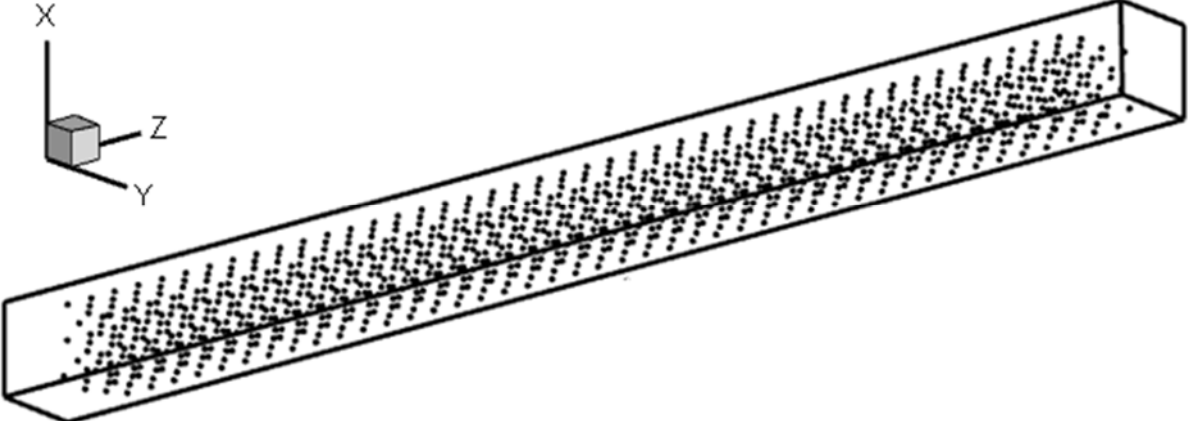
Fig. 7 The mean resuspension velocity (a) in five regions with time development; (b) at the x direction (b) at $t^+=1972$, (c) $t^+=14575$ for 5 to $500\mu m$ particles in the low half of the square duct ($Re_b=36k$, — $5\mu m$, - - - $50\mu m$, - · - · - $100\mu m$, — · — · — $500\mu m$ particles)

Figure 8

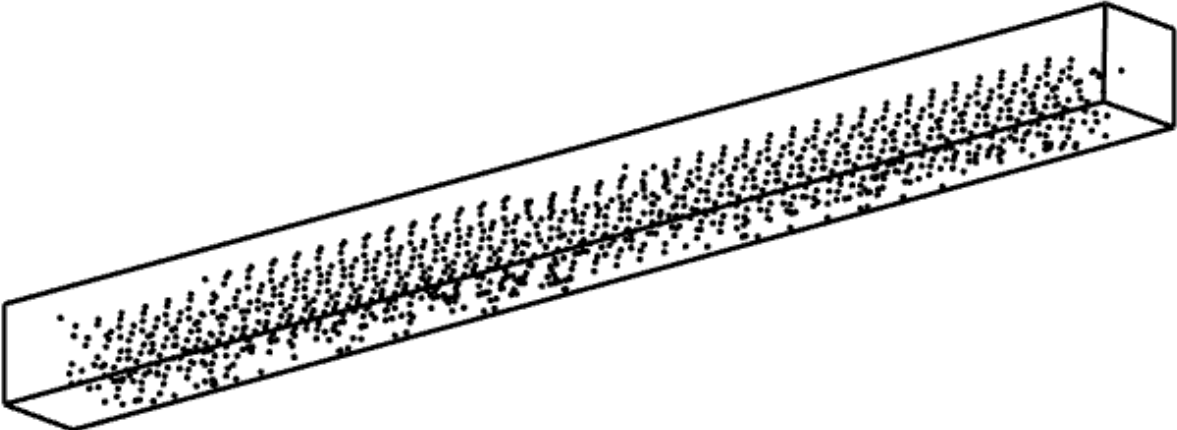


(a)

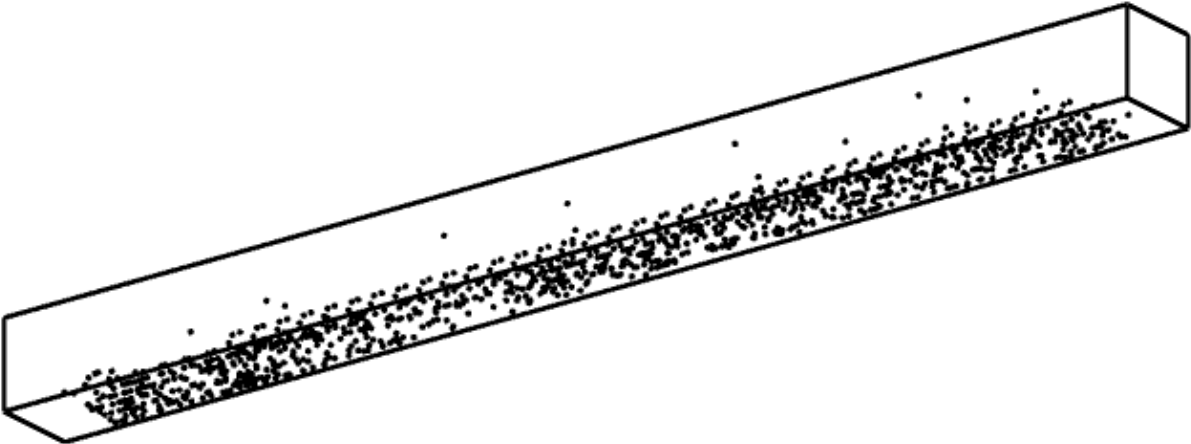
Figure 8 (continued)



$t^+ = 1325$



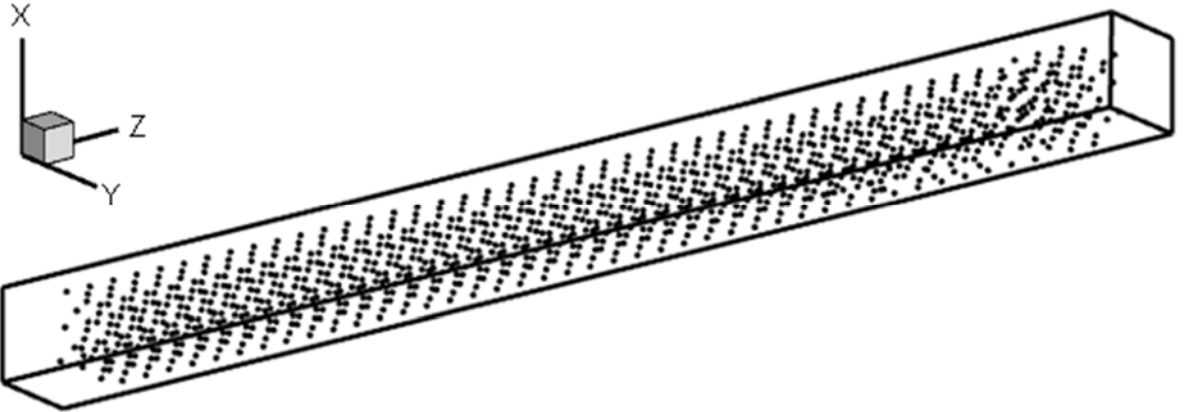
$t^+ = 7780$



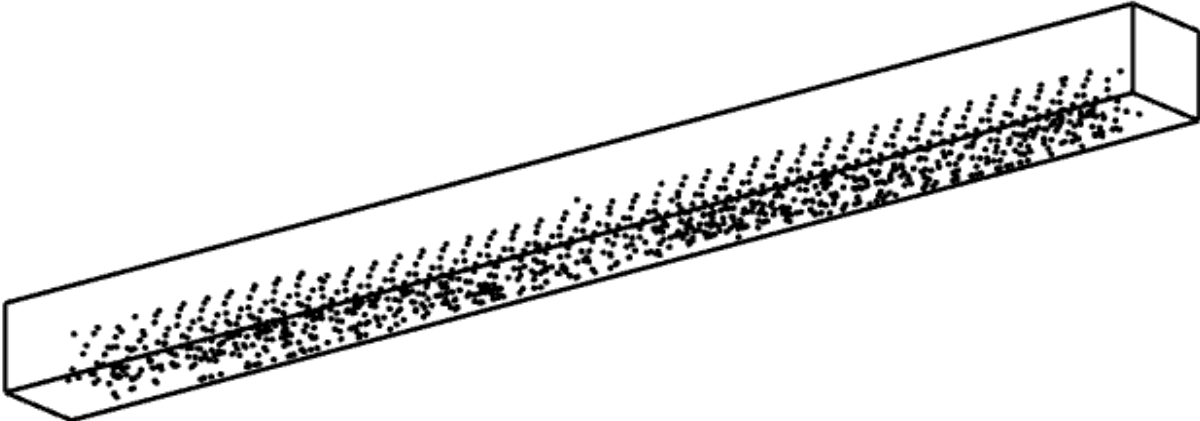
$t^+ = 34450$

(b)

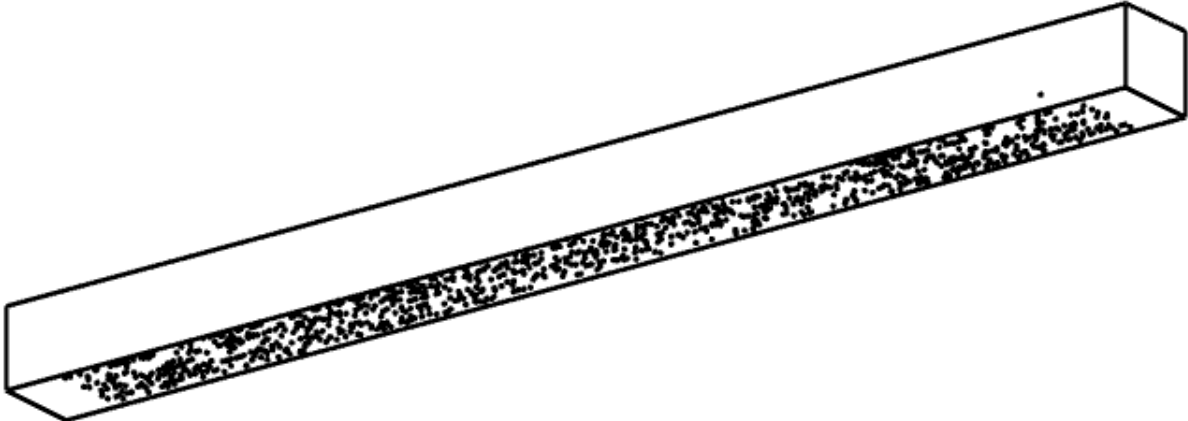
Figure 8 (continued)



$t^+=1325$



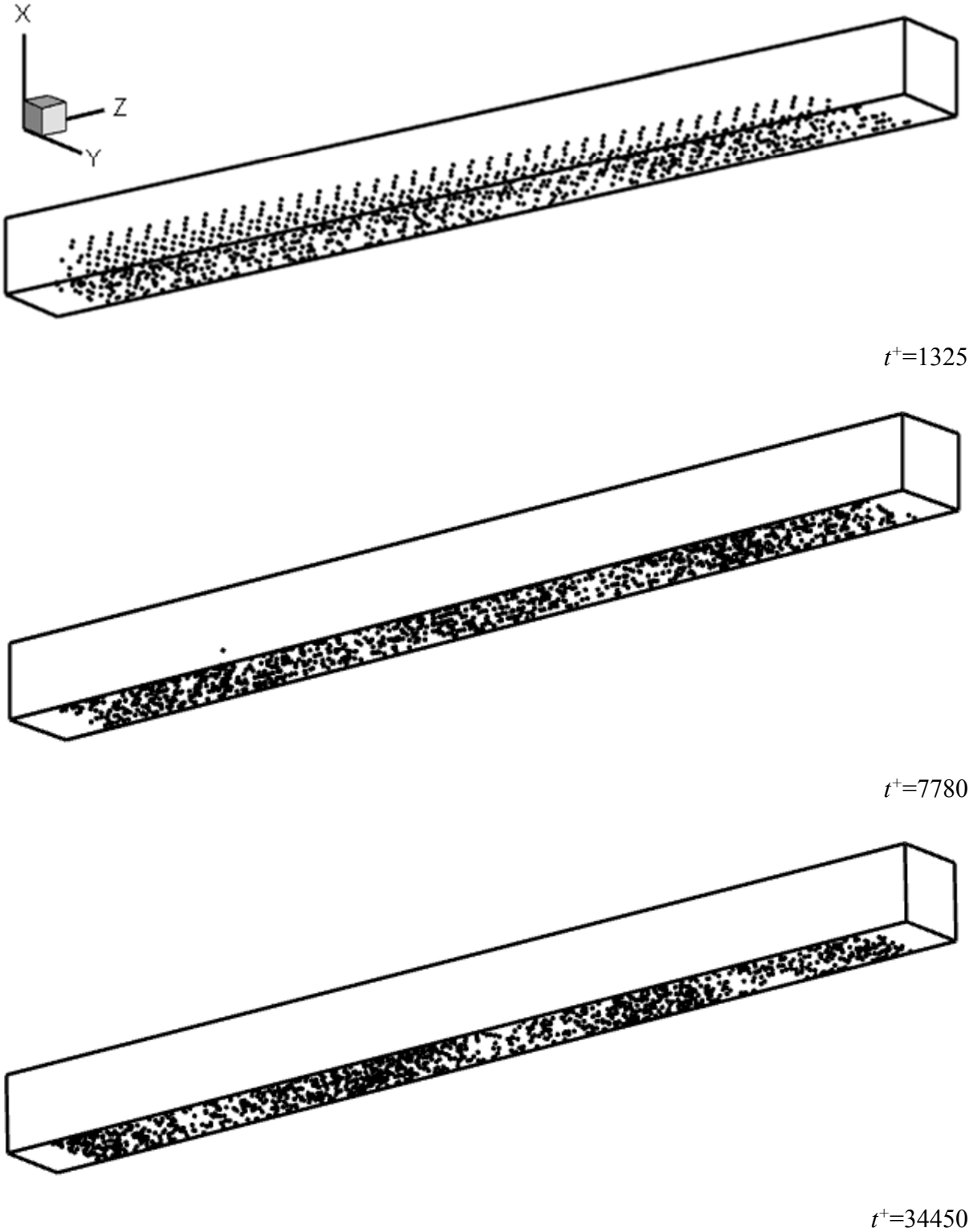
$t^+=7780$



$t^+=34450$

(c)

Figure 8 (continued)



(d)

Fig. 8 Particle trails at $t^+=1325, 7780, 34450$ for particles with (a) 5 (b) 50 (c) 100 (d) $500\mu m$
($Re_b=36k$)

Figure 9

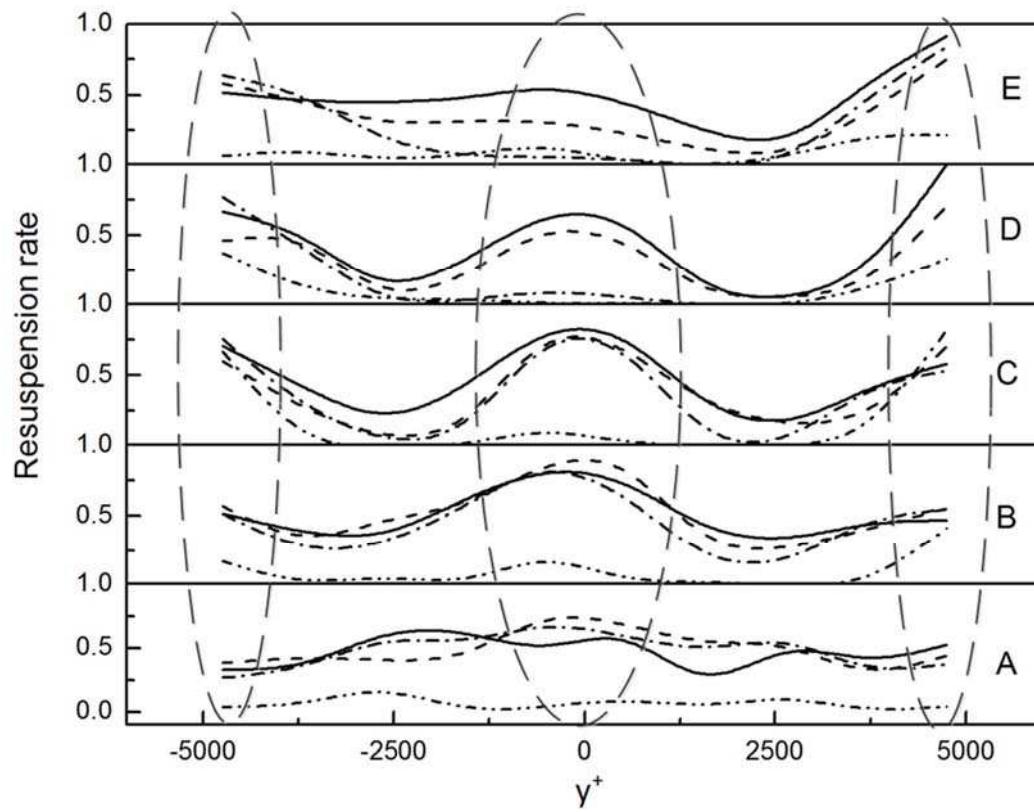
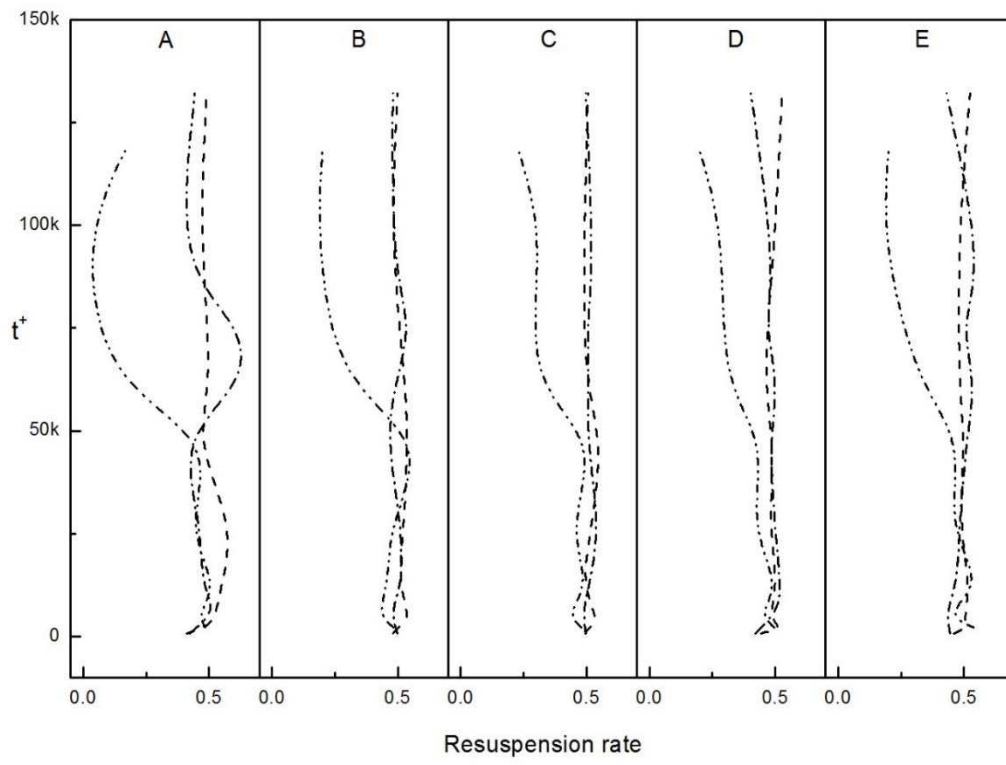
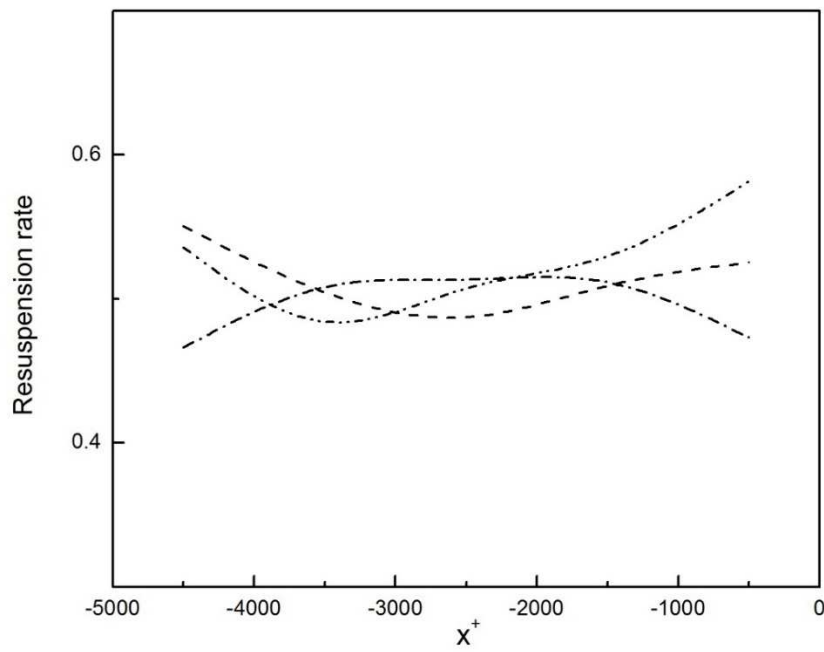


Fig. 9 The distribution of resuspension rate for 5, 50, 100, 500 μm particles in $Re_b=250k$ flow in the lower half duct at $t^+=9139$ (no lift, — $5\mu\text{m}$, - - - $50\mu\text{m}$, - · - · - $100\mu\text{m}$, - - - - $500\mu\text{m}$ particles)

Figure 10

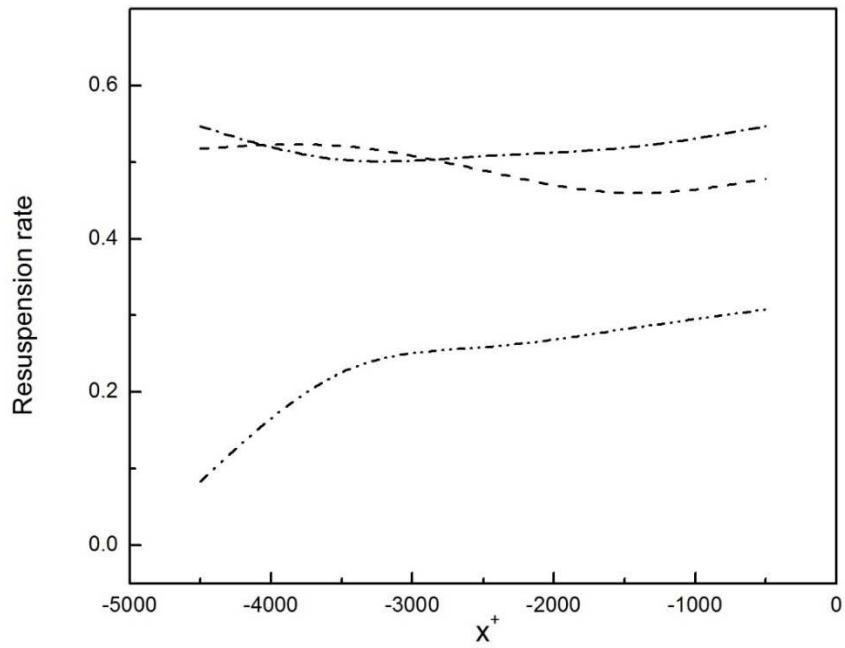


(a)



(b)

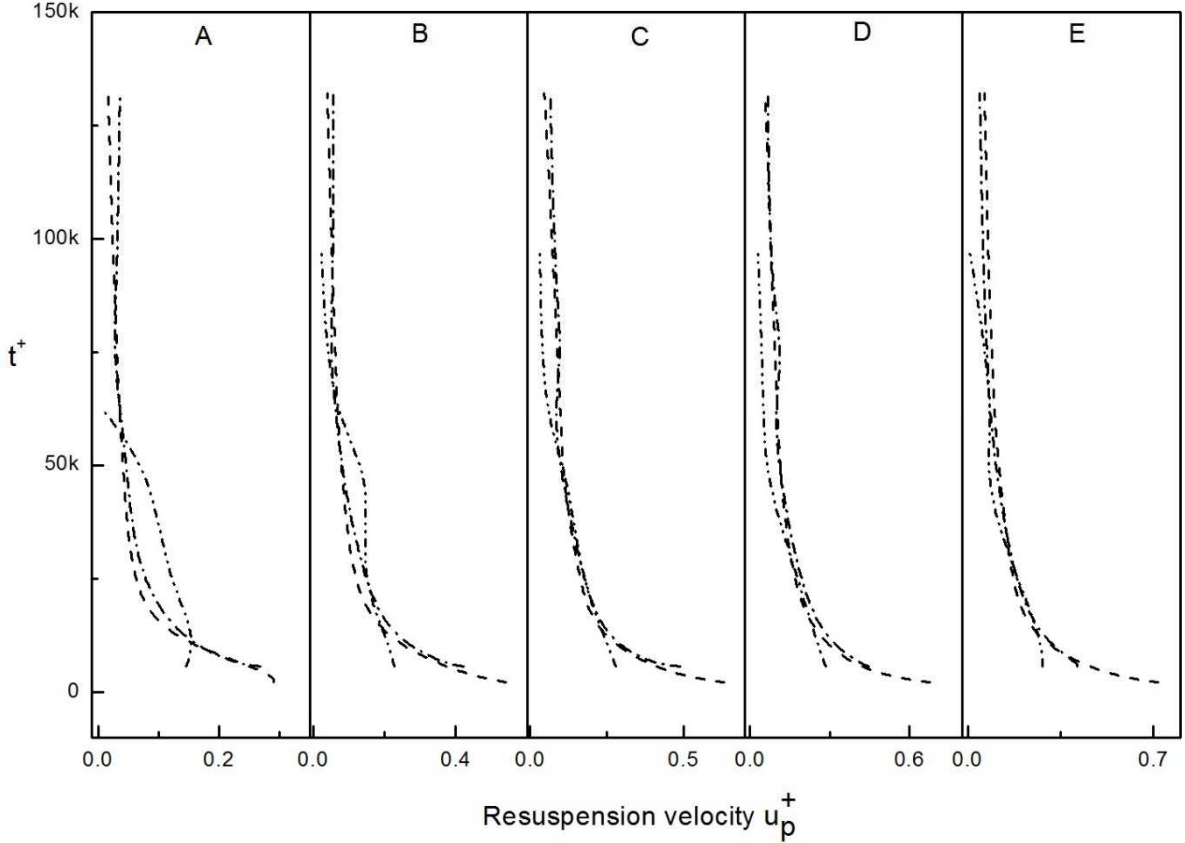
Figure 10 (continued)



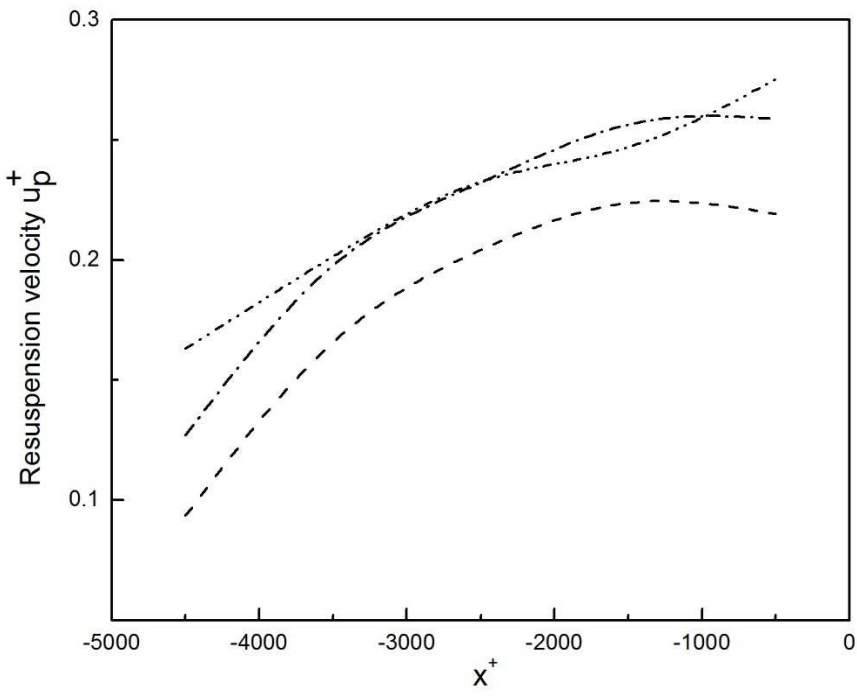
(c)

Fig. 10 (a) Time-dependent mean resuspension rates in five regions, (b) mean resuspension rate profiles along the x direction at $t^+=12654, 61854$ for 50,100,500 μm particles in low half of the duct ($Re_b=250k$, - - - - - 50 μm , - · - · - · 100 μm , · · · · · 500 μm particles).

Figure 11

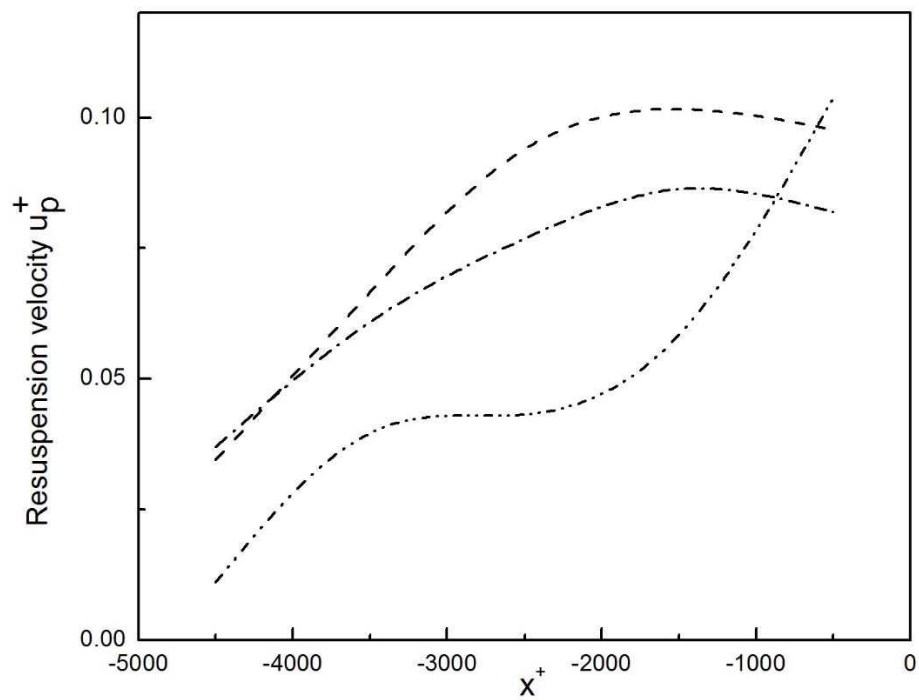


(a)



(b)

Figure 11 (continued)



(c)

Fig. 11 (a) Time-dependent resuspension velocities in five regions; the mean resuspension velocity profiles along the x direction at (b) $t^+=12654$ and (c) $t^+=61854$ for $50, 100, 500\mu m$ particles in low half of the duct ($Re_b=250k$, $-\cdot-\cdot-\cdot-$ $50\mu m$, $-\cdot-\cdot-\cdot-\cdot-$ $100\mu m$, $-\cdot-\cdot-\cdot-\cdot-\cdot-$ $500\mu m$ particles)

Figure 12

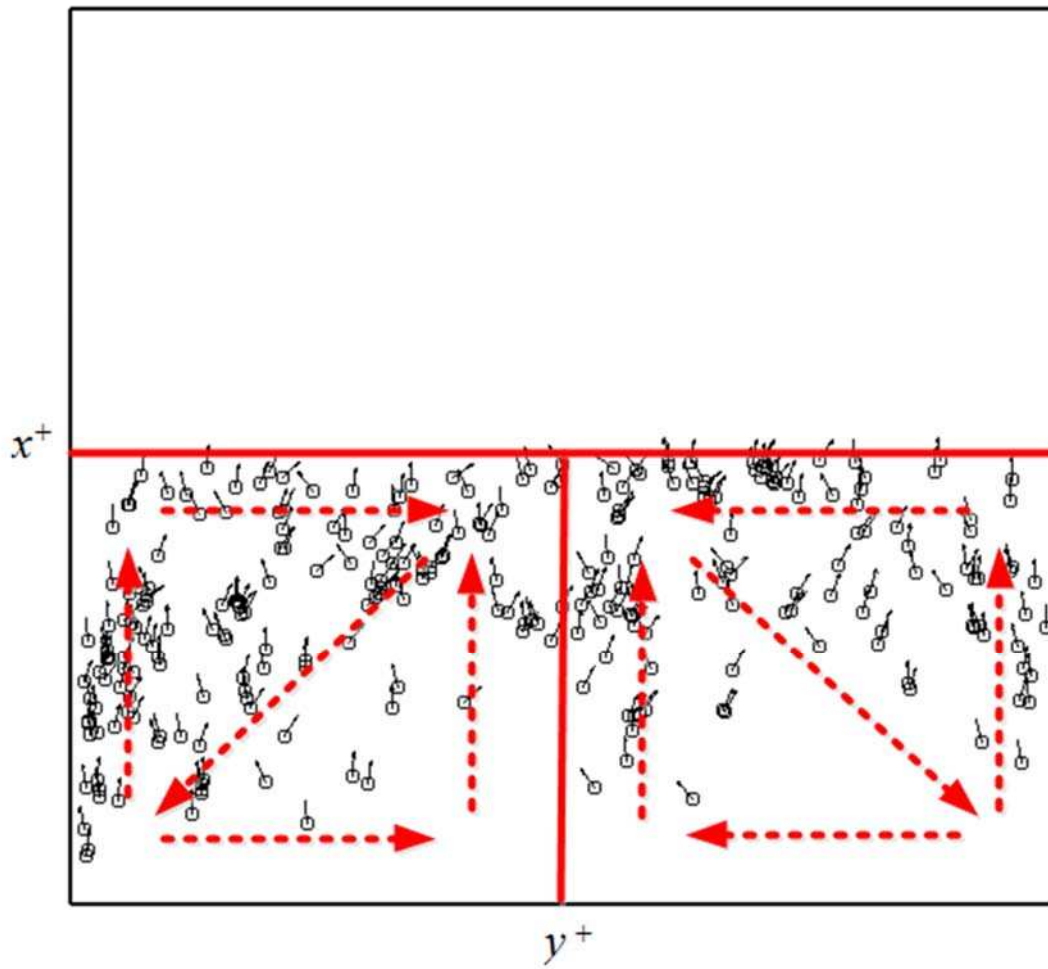


Fig.12 Particle resuspension mechanism in turbulent duct flows

Figure 13

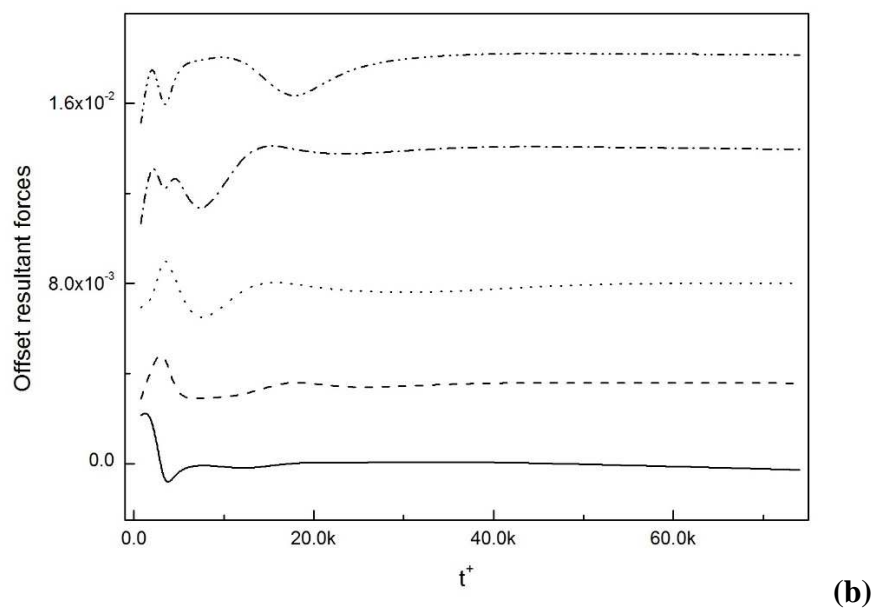
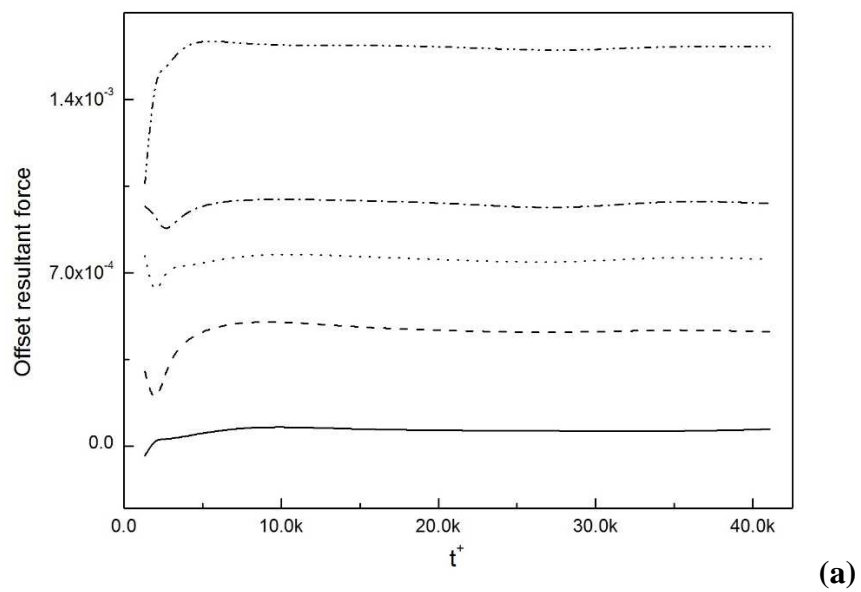
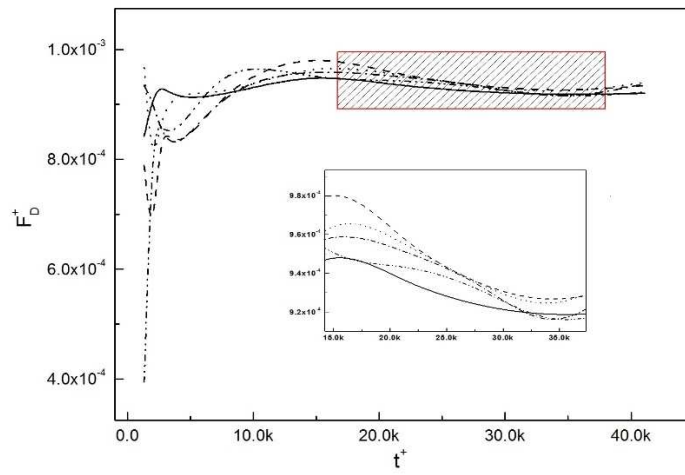
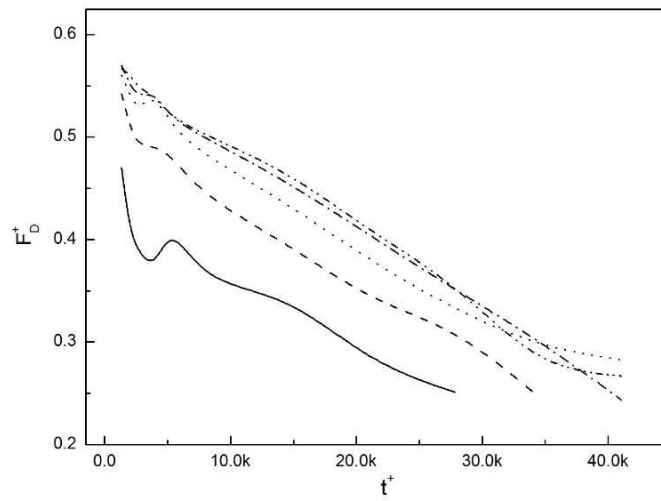


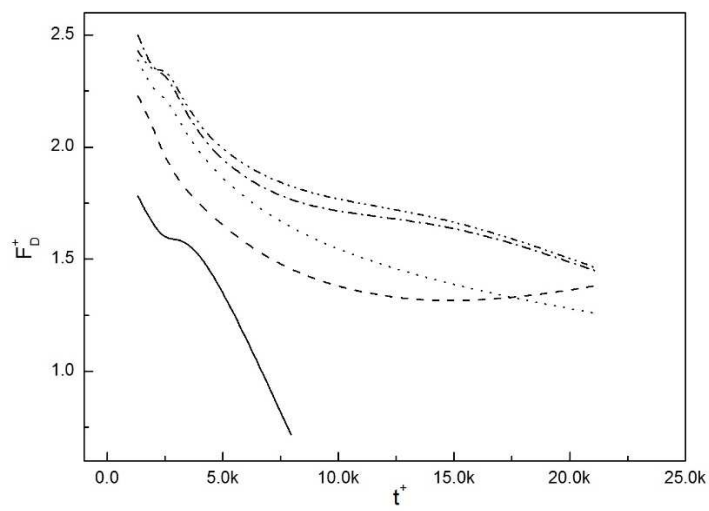
Figure 14



$5 \mu m$



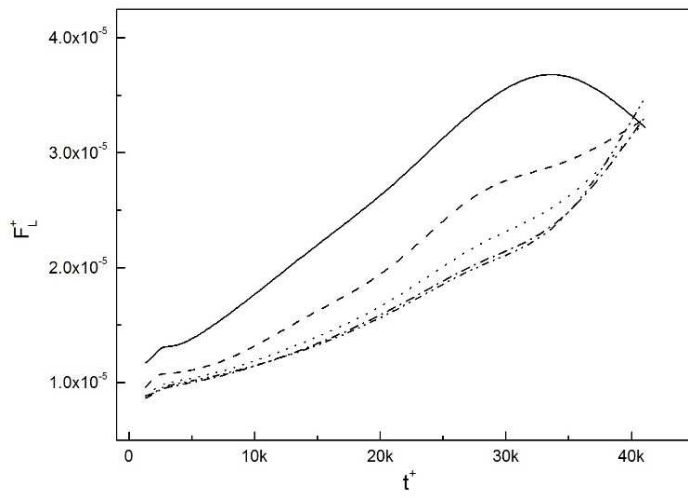
$50 \mu m$



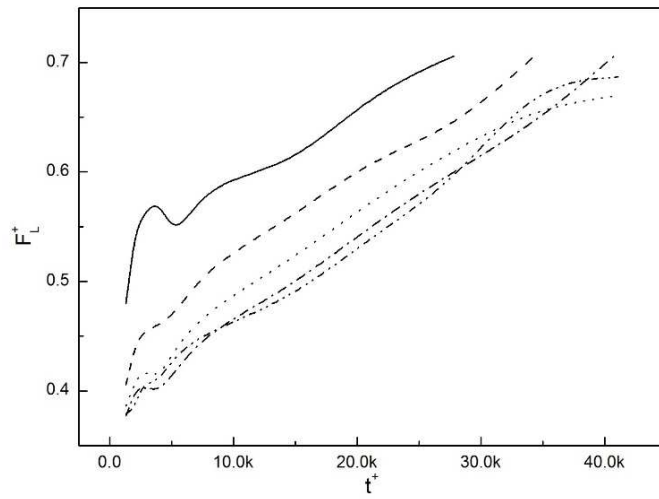
$100 \mu m$

(a)

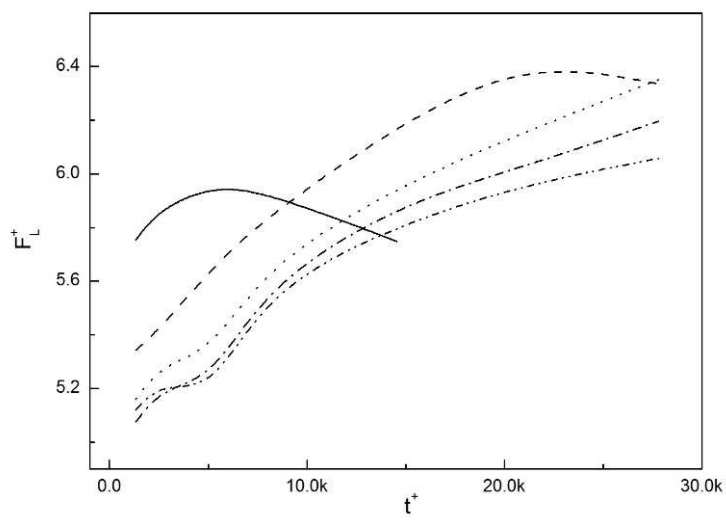
Figure 14 (continued)



$5\mu m$



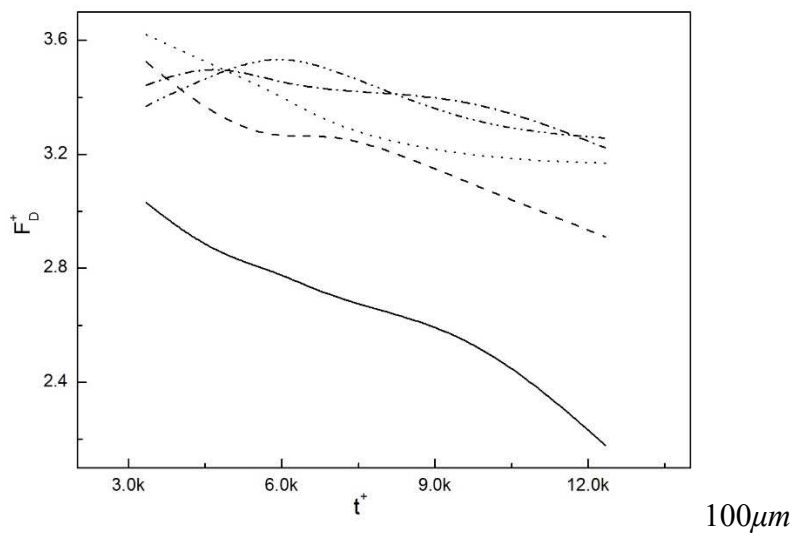
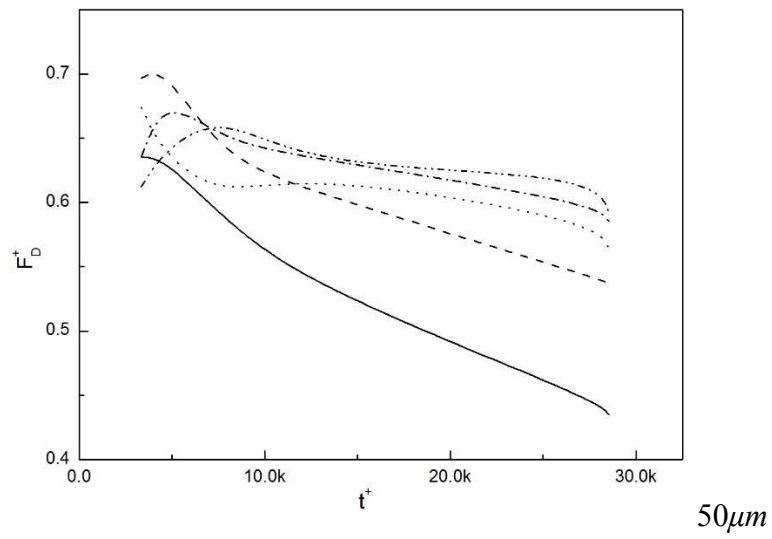
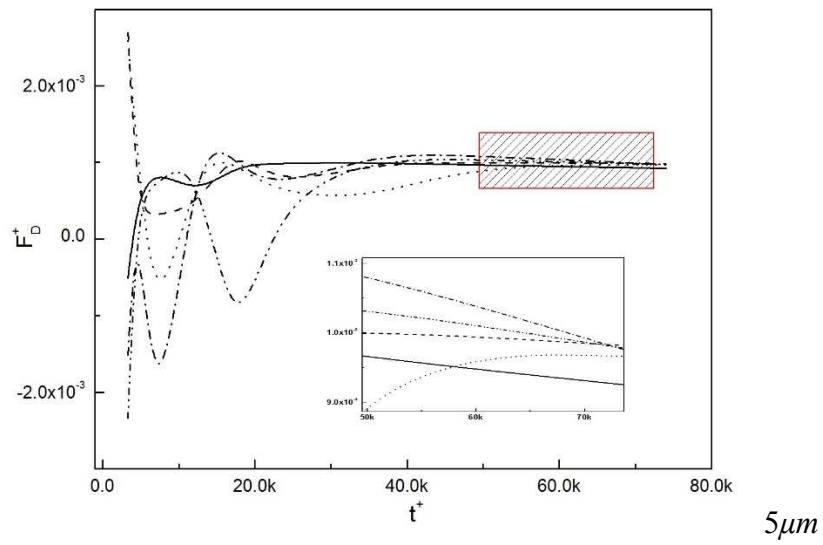
$50\mu m$



$100\mu m$

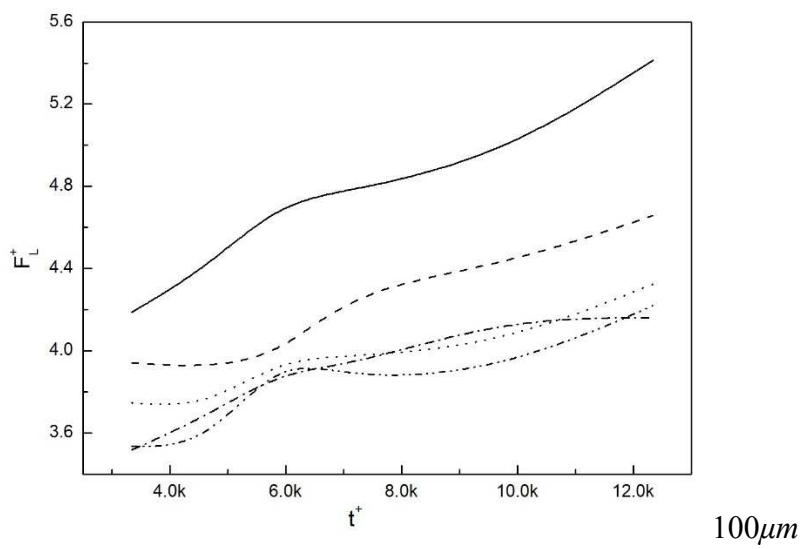
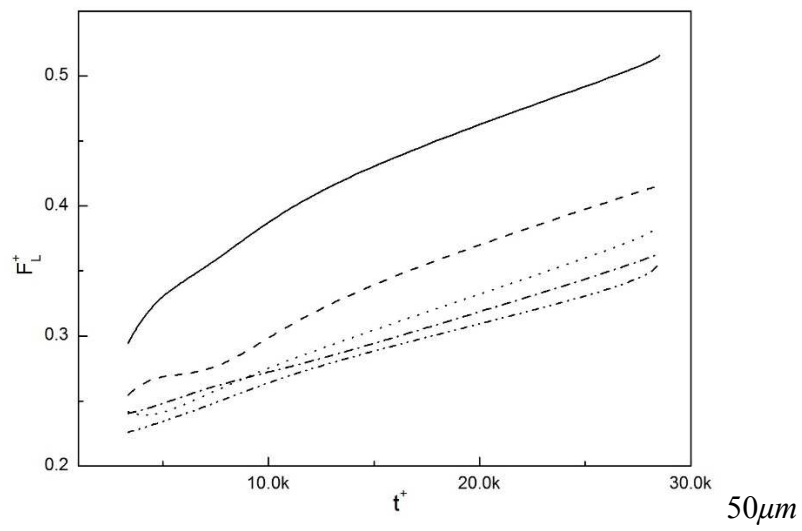
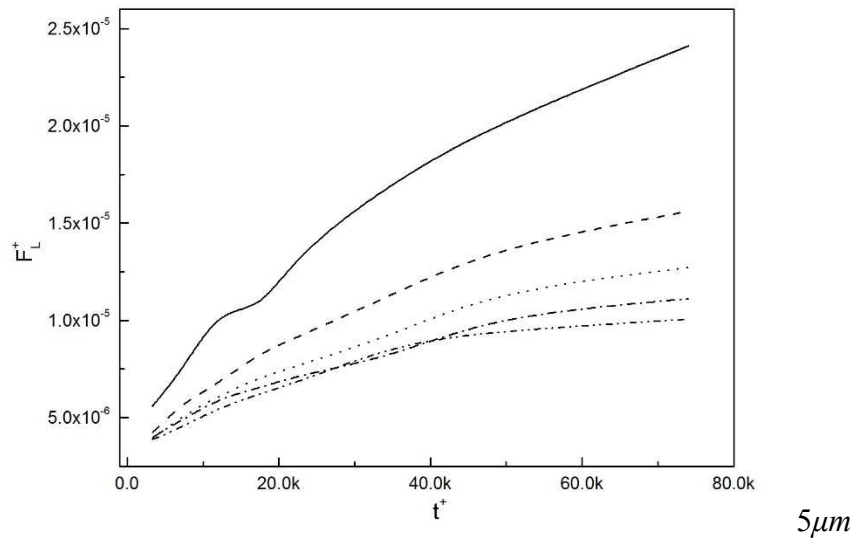
(b)

Figure 14 (continued)



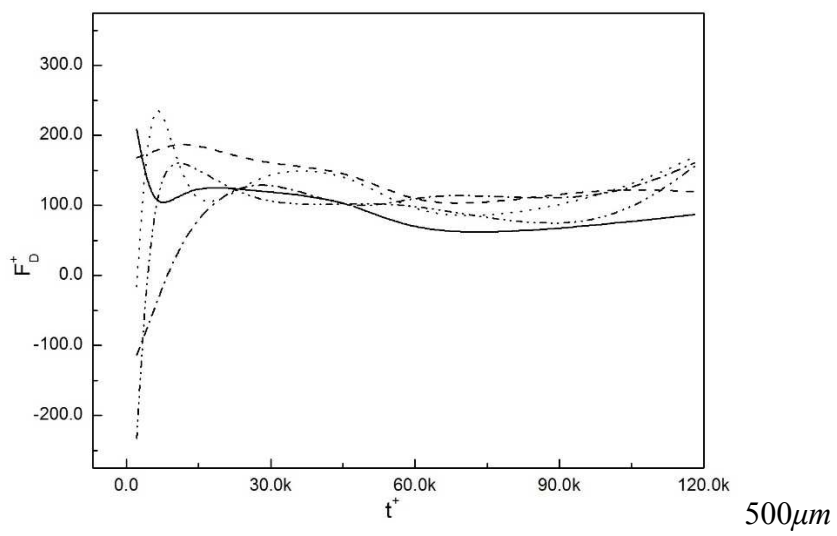
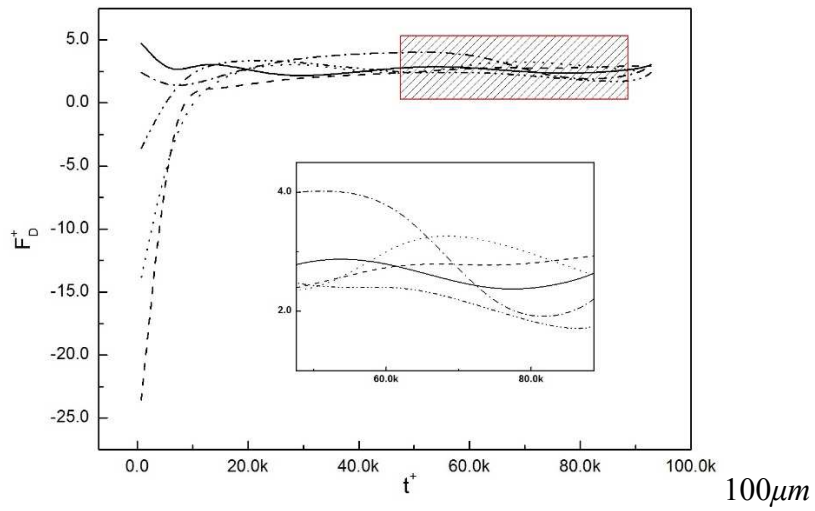
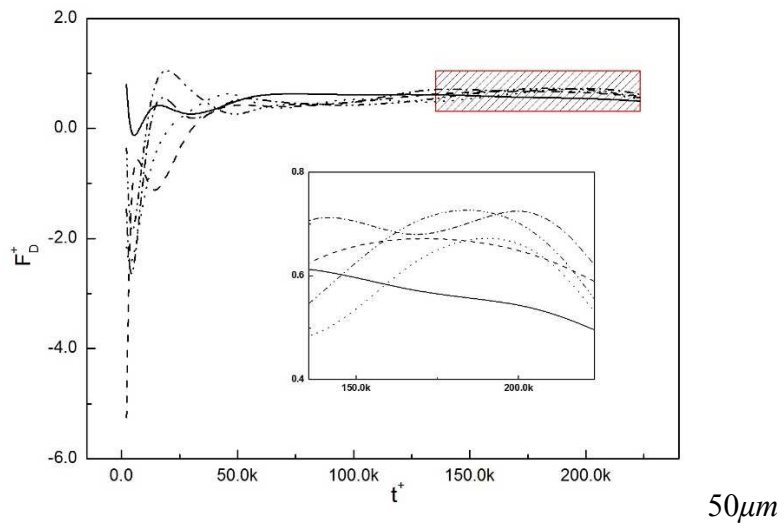
(c)

Figure 14 (continued)



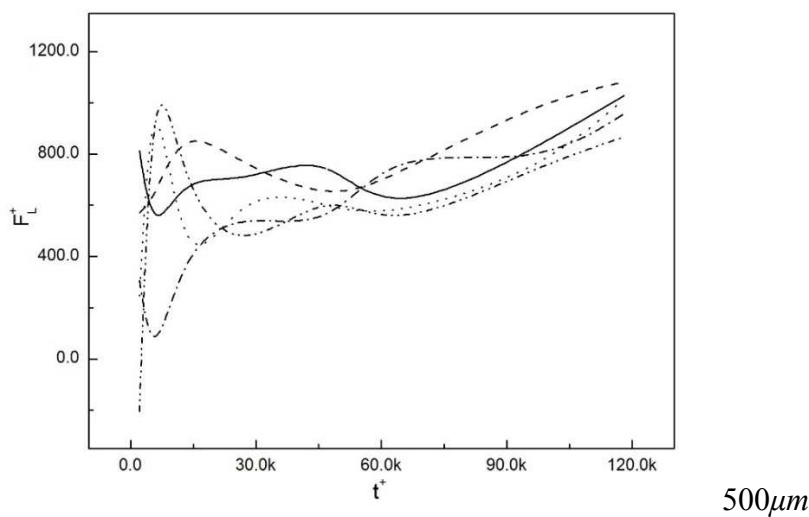
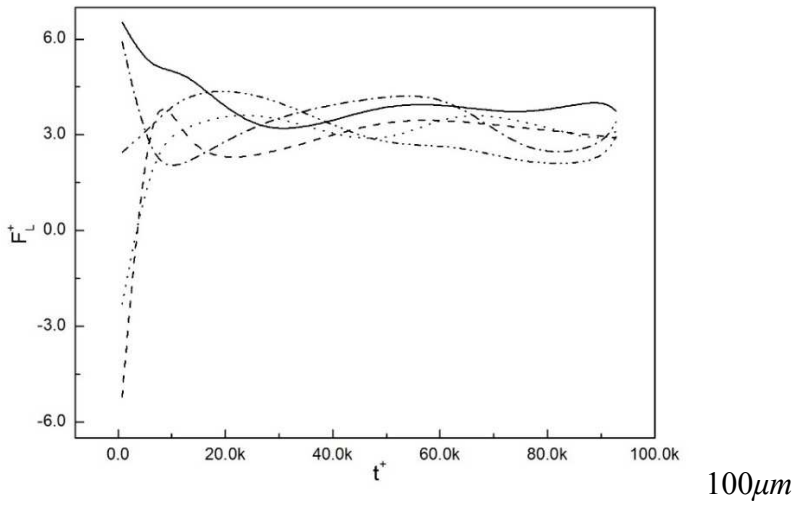
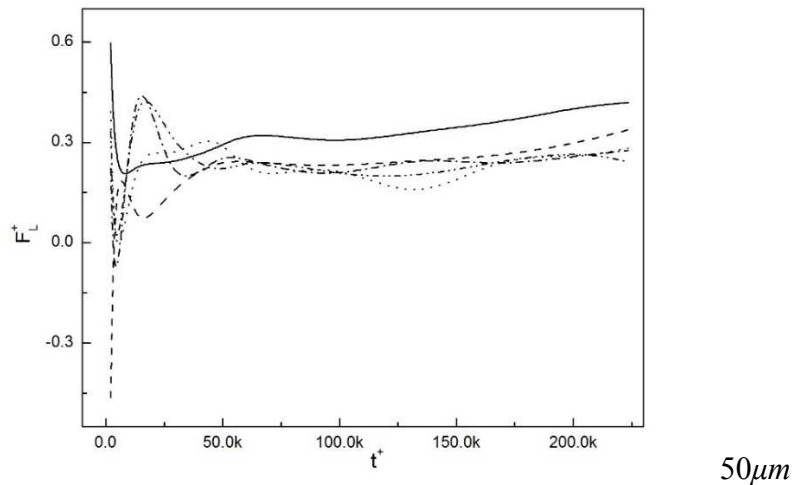
(d)

Figure 14 (continued)



(e)

Figure 14 (continued)



(f)

Fig. 14 Drag force and lift force varying with time for considered particles in $Re_b=36.5k$: (a) drag force, (b) lift force; $Re_b=83k$ (c) drag force, (d) lift force; $Re_b=250k$: (e) drag force, (f) lift force, flow (———— “A”, - - - - - “B”, “C”, - · - · - · “D”, - · - · - · “E”).